Western Kentucky University
TopSCHOLAR®

Masters Theses & Specialist Projects | Graduate School

Spring 2018

Synthesis and Kinetic Studies of High-Valent Metal-Oxo Species Generated by Photochemical and Chemical Methods

Haiyan Liu
Western Kentucky University, haiyanliu2018@gmail.com

Follow this and additional works at: https://digitalcommons.wku.edu/theses

Part of the Organismal Biological Physiology Commons

Recommended Citation
Liu, Haiyan, "Synthesis and Kinetic Studies of High-Valent Metal-Oxo Species Generated by Photochemical and Chemical Methods" (2018). *Masters Theses & Specialist Projects.* Paper 2803.
https://digitalcommons.wku.edu/theses/2803

This Thesis is brought to you for free and open access by TopSCHOLAR®. It has been accepted for inclusion in Masters Theses & Specialist Projects by an authorized administrator of TopSCHOLAR®. For more information, please contact topscholar@wku.edu.

SYNTHESIS AND KINETIC STUDIES OF HIGH-VALENT METAL-OXO SPECIES GENERATED BY PHOTOCHEMICAL AND CHEMICAL METHODS

A Thesis
Presented to
The Faculty of the Department of Chemistry
Western Kentucky University
Bowling Green, Kentucky

In Partial Fulfillment
of the Requirements for the Degree
Master of Science

By
Haiyan Liu

May 2018

SYNTHESIS AND KINETIC STUDIES OF HIGH-VALENT METAL-OXO SPECIES GENERATED BY PHOTOCHEMICAL AND CHEMICAL METHODS

Date Recommended 03-29-2018

Dr. Rui Zhang, Director of Thesis

Dr. Edwin Stevens

Dr. Lawrence Hill

4/23/18

Dean, Graduate Studies and Research Date

ACKNOWLEDGEMENTS

First and foremost, I want to thank my advisor Dr. Rui Zhang. It has been my honor to be his Master of Science student from the fall of 2016 until now. During my study at Western Kentucky University, Dr. Zhang has contributed his time, ideas, and patience to make my M. Sc. experience immensely productive and stimulating. The joy and enthusiasm he exudes in his research is contagious and continued to motivate me even through the toughest times of my M. Sc. pursuit. Regardless of what the future holds for myself or my career, I will always remember how fortunate I am to have been under the guidance of Dr. Zhang.

I am also thankful for the members of Dr. Zhang's research group, who have contributed immensely to my WKU experience, both personally and professionally. Our group has been a source of friendship, good advice, and collaborations. I am especially grateful for the following group members for having stuck it out with me in graduate school: Ka Wai Kwong, Ngo Fung Lee, Dharmesh Patel, Jonathan Malone, Mike Winchester and Davis Ranburger. I would like to acknowledge honorary group member Ka Wai Kwong. Before finishing his study at WKU, Ka Wai Kwong gave me excellent laboratory training, for which I have sincere gratitude. I want to thank Ngo Fung Lee, who worked with me on the metal(IV)-oxo porphyrin experiments. I very much appreciated Ngo Fung Lee's enthusiasm, integrity, and willingness to help me in the

research laboratory. The NMR analysis studies discussed in this dissertation would not have been possible without the tremendous support of Dr. Lester Pesterfield and Dr. Kevin Williams. I would like to thank the other two members of my defense committee, Dr. Lawrence Hill and Dr. Edwin Stevens, for their time and insightful questions. I want to thank Ms. Alicia Pesterfield for chemical supply. I would like to thank Ms. Haley Smith from the Office of Chemistry Department for patiently answering all my various questions.

In closing, I would like to thank my elder sister Anita Tucker and brother-in-law Jesse Tucker, for all their love and encouragement. Most of all, I give thanks to my husband Xinming Shi and my lovely daughter Ziyu Shi for their faithful support and encouragement throughout my entire duration of study in the United States.

Haiyan Liu

May 2018

TABLE OF CONTENTS

CHAPTER 1 INTRODUCTION.....1

1.1 General introduction of cytochrome P450 enzymes.....1

1.2 Compound I and compound II species.....6

1.3 Biomimetic oxidation by metalloporphyrins.....8

1.4 Photochemical generation of high-valent metal-oxo species.....10

CHAPTER 2 EXPERIMENTAL SECTION.....13

2.1 Materials.....13

2.2 Methods.....14

2.2.1 Physical measurement.....14

2.2.2 Pyrrole purification.....15

2.2.3 General procedure for photolysis of porphyrin iron(III) bromate

$[Fe^{III}(Por)(BrO_3)]$ (4**a** - 4**b**) 15

2.2.4 General procedure for photolysis of porphyrin manganese(III) chlorates [Mn^{III}(Por)(ClO_3) (5**a** - 5**b**) 16

2.2.5 Direct kinetic study of high-valent iron-oxo intermediates.....16

2.2.6 General procedure for catalytic competition studies 17

2.3 Synthesis and characterization.....18

2.3.1 Synthesis of 5,10,15,20-tetrakis(2,6-dichlorophenyl) porphyrin [H_2(TDCPP)] (**1a**) and 5,10,15,20-tetrakis(2,6-difluorophenyl) porphyrin [H_2(TDFPP)] (**1b**) 18

2.3.2 Synthesis of iron(III) porphyrin chloride [Fe^{III}(Por)Cl] and manganese(III) porphyrin chloride [Mn^{III}(Por)Cl] 22

CHAPTER 3 IRON(IV)-OXO AND MANGANESE(IV)-OXO PORPHYRIN SPECIES GENERATED BY PHOTOCHEMICAL AND CHEMICAL METHODS.....28

3.1 Introduction.....28

3.2 Generation of porphyrin-iron(IV)-oxo species.....29

3.2.1 Chemical generation of porphyrin-iron(IV)-oxo complexes….....29

3.2.2 Photochemical generation of iron(IV)-oxo porphyrins.....31

3.3 Generation of porphyrin-manganese(IV)-oxo species.....35

3.3.1 Chemical generation of porphyrin-manganese(IV)-oxo species.....35

3.3.2 Photochemical generation of porphyrin-manganese(IV)-oxo species.....37

CHAPTER 4 KINETIC STUDIES OF IRON(IV)-OXO COMPOUND II SPECIES....40

4.1 Introduction.....40

4.2 Kinetic studies of epoxidation and hydroxylation by iron(IV)-oxo (**6a**-**b**) generated by photochemical and chemical methods 41

4.3 Kinetic studies of sulfoxidation by photo-generated compound II models [Fe^{IV}(Por)O] (**6a**-**b**)….....46

4.4 Competition studies of sulfide oxidation reactions.....51

CHAPTER 5 CONCLUSION.....57

LIST OF FIGURES

Figure 1. Iron(III) protoporphyrin IX linked with a proximal cysteine ligand.....3

Figure 2. X-ray structure of $CYP450_{cam}$.....5

Figure3. Agilent 8454 diode array UV-visible spectrophotometer (right) and Sola light engine (left).....14

Figure 4. (A) The UV-vis spectrum of [H_2(TDCPP)] (**1a**) in CH_2Cl_2; (B) The ^{1}H-NMR spectrum of [H_2(TDCPP)] (**1a**) in $CDCl_3$.....21

Figure 5. (A) The UV-vis spectrum of [H_2(TDFPP)] (**1b**) in CH_2Cl_2; (B) The ^{1}H-NMR spectrum of [H_2(TDFPP)] (**1b**) in $CDCl_3$.....21

Figure 6. (A) The UV-vis spectrum of [Fe^{III}(TDCPP)Cl] (**2a**) in CH_2Cl_2; (B) The ^{1}H-NMR spectrum of [Fe^{III}(TDCPP)Cl] (**2a**) in $CDCl_3$.....25

Figure 7. (A) The UV-vis spectrum of [Fe^{III}(TDFPP)Cl] (**2b**) in CH_2Cl_2; (B) The ^{1}H-NMR spectrum of [Fe^{III}(TDFPP)Cl] (**2b**) in $CDCl_3$.....26

Figure 8. (A) The UV-vis spectrum of [Mn^{III}(TDCPP)Cl] (**3a**) in CH_2Cl_2; (B) The

^{1}H-NMR spectrum of [Mn^{III}(TDCPP)Cl] (**3a)** in $CDCl_3$.....26

Figure 9. (A) The UV-vis spectrum of [Mn^{III}(TDFPP)Cl] (**3b**) in CH_2Cl_2; (B) The

^{1}H-NMR spectrum of [Mn^{III}(TDFPP)Cl] (**3b**) in $CDCl_3$.....27

Figure 10. (A) Time-resolved spectra of forming [Fe^{IV}(TDCPP)O] (**6a**) by

[Fe^{III}(TDCPP)Cl] (**2a**) react with 5 equiv. of $PhI(OAc)_2$; (B) Time-resolved spectra of

forming [Fe^{IV}(TDFPP)O] (**6b**) by [Fe^{III}(TDFPP)Cl] (**2b**) react with 5 equiv. of

$PhI(OAc)_2$.....30

Figure 11. (A) Time-resolved spectra for forming of photo-generated [Fe^{IV}(TDCPP)O]

(**6a**); (B)Time-resolved spectra for forming of photo-generated [Fe^{IV}(TDFPP)O] (**6b**)

.....33

Figure 12. (A) Time-resolved spectra of forming [Mn^{IV}(TDCPP)O] (**7a**) by

[Mn^{III}(TDCPP)Cl] (**3a**) react with 30 equiv. of $PhI(OAc)_2$; (B)Time-resolved spectra of

forming [Mn^{IV}(TDFPP)O] (**7b**) by [Mn^{III}(TDCPP)Cl] (**3b**) react with 30 equiv. Of

$PhI(OAc)_2$.....36

Figure 13. (A) Axial ligand exchange of [Mn^{III}(TDCPP)Cl] (**3a**) with $AgClO_3$; monitored

by UV-vis spectroscopy: [Mn^{III}(TDCPP)Cl] (**3a**) (dashed) and [Mn^{III}(TDCPP)ClO_3] (**5a**)

(solid); (B) Axial ligand exchange of [Mn^{III}(TDFPP)Cl] (**3b**) with $AgClO_3$; monitored by UV-vis spectroscopy: [Mn^{III}(TDFPP)Cl] (dashed) and [Mn^{III}(TDFPP)ClO_3] (**5b**) (solid).....38

Figure 14. (A) Time-resolved spectra for forming photo-generated [Mn^{IV}(TDCPP)O] (**7a**); (B) Time-resolved spectra for forming photo-generated [Mn^{IV}(TDFPP)O] (**7b**) 39

Figure 15. (A) Time-resolved spectra of oxidation reaction of photo-generated [Fe^{IV}(TDCPP)O] (**6a**) with *c*is-stilbene (70 mM); (B) Time-resolved spectra of oxidation Reaction of chemical-generated [Fe^{IV}(TDCPP)O] (**6a**) with *c*is-stilbene (70 mM) 42

Figure 16. (A) Time-resolved spectra for reaction of photo-generated [Fe^{IV}(TDFPP)O] (**6b**) with *c*is-cyclooctene (0.4 M); (B) Time-resolved spectra for reaction of chemical-generated [Fe^{IV}(TDCPP)O] (**6b**) with *c*is-cyclooctene (0.4 M) 43

Figure 17. (A) Kinetic plots of the observed rate constants for the reaction of photo-generated (**6a**) versus the concentration of *c*is-stilbene, 4-methylstyrene and diphenylmethane; (B) Kinetic plots of the observed rate constants for the reaction of chemical-generated (**6a**) versus the concentration of *c*is-stilbene, 4-methylstyrene and diphenylmethane.....44

Figure 18. (A) Time-resolved spectra of photo-generated **6a** reacting in CH_3CN with

thioanisole (0.4 M) over 60 s. (B) Kinetic plots of the observed rate constants for the reaction of **6a** versus the concentration of thioanisole.....47

Figure 19. Hammett correlation studies (log k_{rel} vs σ^+) for the Fe^{III}(TDFPP)Cl-catalyzed oxidation of substituted thioanisoles by $PhI(OAc)_2$ in CH_3CN at 23 ± 2 °C.....56

LIST OF SCHEMES

Scheme 1. Cytochrome P450s monooxygenase reaction (S = substrate) 2

Scheme 2. Oxidations catalyzed by cytochrome P450s enzymes.....4

Scheme 3. Stereospecific hydroxylation of the *exo* C-H bond at position 5 of camphor by $CYP450_{cam}$.....5

Scheme 4. Chemical generation of compound I and compound II species.....8

Scheme 5. Typical metalloporphyrin-mediated reactions.....9

Scheme 6. Photo-induced ligand cleavage reactions for production of high-valent transition metal-oxo species.....12

Scheme 7. Two-step synthesis of [H_2(TDCPP)] (**1a**) and [H_2(TDFPP)] (**1b**) 18

Scheme 8. Synthesis of [Fe^{III}(Por)Cl] (**2a-b**) 22

Scheme 9. Synthesis of [Mn^{III}(Por)Cl] (**3a-b**) 23

Scheme 10. Chemical generation of iron(IV)-oxo species (**6a-b**) 29

Scheme 11. Photochemical formation of porphyrin-iron(IV)-oxo complexes (**6a-b**).....31

Scheme 12. Chemical generation of manganese(IV)-oxo species (**7a-b**) 35

Scheme 13. Photochemical formation of porphyrin-manganese(IV)-oxo (**7a-b**) complexes by visible light irradiation of manganese chlorate salts (**5a-b**) 37

Scheme 14. A disproportionation pathway for reactions of species **6**.....50

Scheme 15. Iron(III) porphyrin-catalyzed sulfide oxidations with $PhI(OAc)_2$.....52

LIST OF TABLES

Table 1. Second-order rate constants for reactions of porphyrin-iron(IV)-oxo species **6** ……...45

Table 2. Second-order rate constants (k_{ox}) for reactions of porphyrin-iron(IV)-oxo species 6.....48

Table 3. Relative rate constants from kinetic studies and competition catalytic oxidation 54

SYNTHESIS AND KINETIC STUDIES OF HIGH-VALENT METAL-OXO SPECIES GENERATED BY PHOTOCHEMICAL AND CHEMICAL METHODS

Haiyan Liu May 2018 Pages 71

Directed by: Dr. Rui Zhang, Dr. Edwin Stevens, Dr. Lawrence Hill

Department of Chemistry Western Kentucky University

Highly reactive iron-oxo intermediates play important roles as active oxidants in enzymatic and synthetic catalytic oxidation. Many transition metal catalysts are designed for biomimetic studies of the predominant oxidation catalysts in Nature, namely cytochrome P450 enzymes. In this work, a series of iron(IV)-oxo porphyrins [Fe^{IV}(Por)O] and manganese(IV)-oxo porphyrins [Mn^{IV}(Por)O] have been successfully produced in two electron-deficient ligands by photochemical and chemical methods, and spectroscopically characterized by UV-vis, and ^{1}H-NMR.

With iodobenzene diacetate [PhI$(OAc)_2$] as the oxygen source, iron(III) porphyrin and manganese(III) porphyrin complexes converted to the corresponding metal(IV)-oxo species as oxygen atom transfer (OAT) agents. In addition, a new photochemical method was developed to generate the same species by visible light irradiation of highly photo-labile porphyrin-iron(III) bromate or porphyrin-manganese(III) chlorate precursors. Furthermore, the kinetics of oxygen transfer atom reactions with alkene, active hydrocarbons and aryl sulfides by photo-generated and chemical-generated [Fe^{IV}(Por)O]

were studied in CH_3CN solutions. Apparent second-order rate constants determined under pseudo-first-order conditions for sulfide oxidation reactions are $(9.8 \pm 0.1) \times 10^2 - (3.7 \pm 0.3) \times 10^1$ $M^{-1}s^{-1}$, which are 3 to 4 orders of magnitude greater in comparison with those of alkene epoxidations and activated C-H bond oxidations by the same oxo species.

CHAPTER 1

INTRODUCTION

1.1 General introduction of cytochrome P450 enzymes

An important technology in synthetic organic chemistry is catalytic oxidation. This process is the key to many fundamental transformations in Nature.[1] Oxidation reactions are applied worldwide to produce oxygenated chemical.[2] Unfortunately, traditional oxidation reactions are performed with prodigious amounts of expensive and/or toxic heavy metals, generate large amounts of waste and give low selectivity.[3] Therefore, there is an increasing demand for catalytic oxidations that employ transition metal catalysts with environmentally friendly oxygen sources. Logically, a significant goal in oxidation chemistry and industry involves oxygen sources such as hydrogen peroxide or molecular oxygen for selective oxidations.[3b, 4] Many transition metal catalysts have been synthesized to mimic the metalloenzymes found in Nature, notably the cytochrome P450 enzymes.

Cytochrome P450 is an enzyme super family, which has been found in all types of life forms, including plants, bacteria and mammals.[1] It consists of two protein components : Cytochrome P450 and a flavoprotein, NADPH. Until now, over 12,000 CYP450s geno isomers have been identified. CYP450 enzymes are heme-containing proteins that often hydrolyze many organic molecules in animals, and play key roles in

catalytic oxidation and biotransformation.[5] Biochemical systems involve oxidative enzymes accelerating catalytic oxidation processes, which are fundamental in many biosynthesis and biodegradation processes.[6] A large majority of these biological oxidations are mediated by heme-containing oxygenates. The most prominent of these oxygenates is the ubiquitous cytochrome P450 monooxygenase (CYP450s) discovered more than 60 years ago. The CYP450s activate molecular oxygen, transferring one oxygen atom into a substrate. This activation reduces the second oxygen to a water molecule, utilizing two electrons provided by electron donors. The donors include NADH or NADPH, via an electron transport protein (Scheme 1). Since only one of the two oxygen atoms from the molecular oxygen has been used and remains in the oxidized substrate, the CYP450s are also termed as monooxygenase.

$$S + O_2 + 2e^- + 2H^+ \xrightarrow{\text{cytochrome P450s}} SO + H_2O$$

Scheme 1. Cytochrome P450s monooxygenase reaction (S = substrate).

It is well known that heme-contain iron may act as a source of electrons for reduction or oxidation reactions. All cytochrome P450 enzymes contain an active site consisting of the iron protoporphyrin IX complex, which is linked to protein via a sulfur

atom of a proximal cysteine ligand (Figure 1). The CYP450s are known to catalyze a large number of oxidations, including epoxidation, hydroxylation, dealkylation, sulfoxidation, dehydrogenation and others oxidations (Scheme 2).[7]

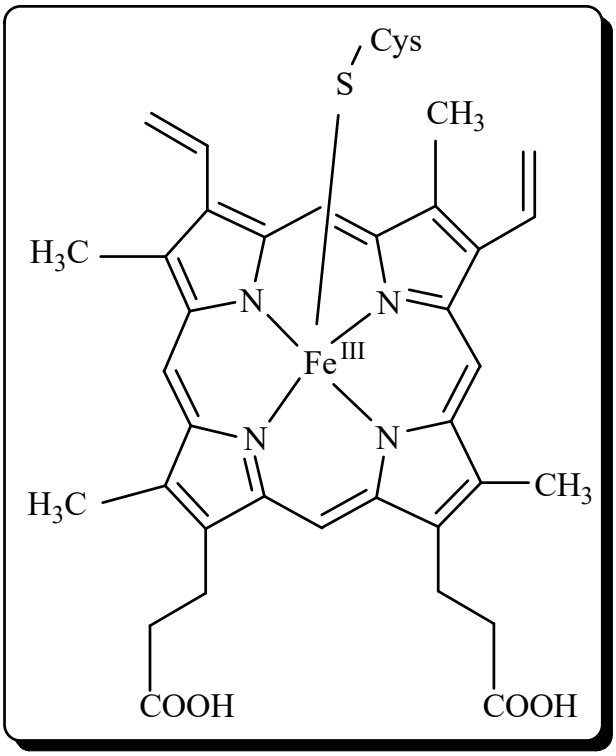

Figure 1. Iron(III) protoporphyrin IX linked with a proximal cysteine ligand.

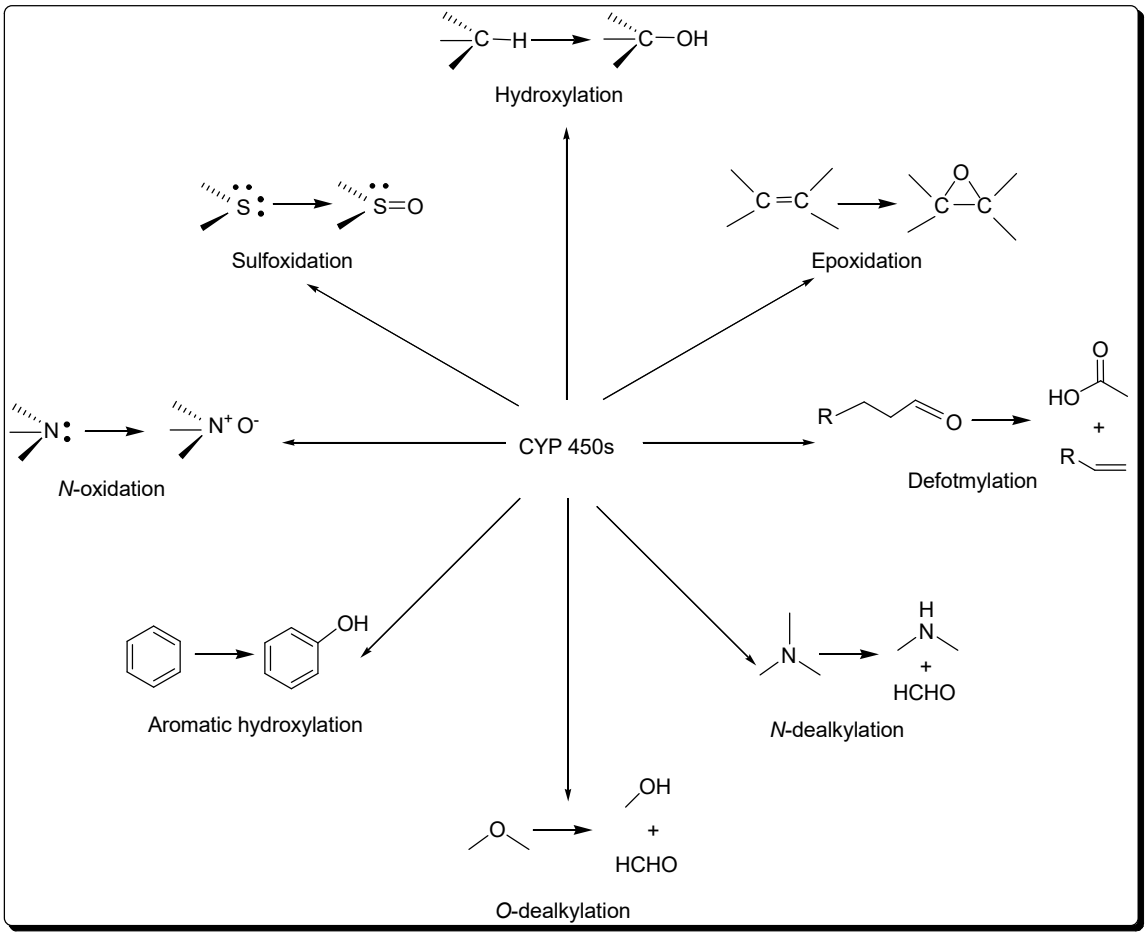

Scheme 2. Oxidations catalyzed by cytochrome P450 enzymes.

In 1986, the X-ray structure of $CYP450_{cam}$ was determined by Poulos and co-workers, which contains a single ferric protoporphyrin-IX complex and a cysteine as an axial ligand (Figure 2).[8] The catalytic hydroxylation by $CYP450_{cam}$ from *Pseudomonas Putida,* with the substrate camphor is shown in Scheme 3. $CYP450_{cam}$ catalyzes the regio-, chemo, and stereospecific hydroxylation of camphor with atmospheric molecular oxygen to yield 5-*exo*-hydroxycamphor.

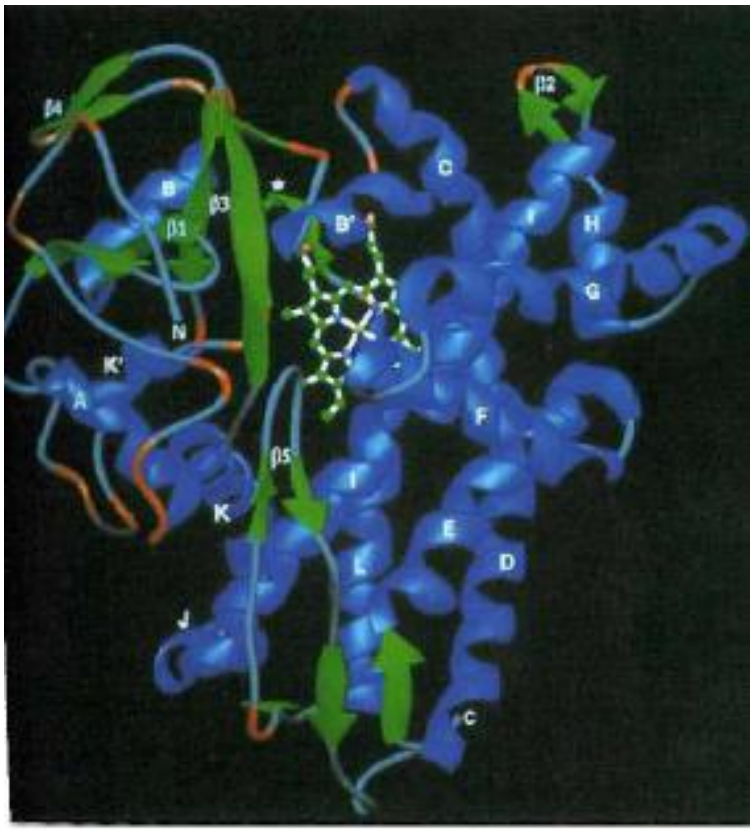

Figure 2. X-ray structure of $CYP450_{cam}$.

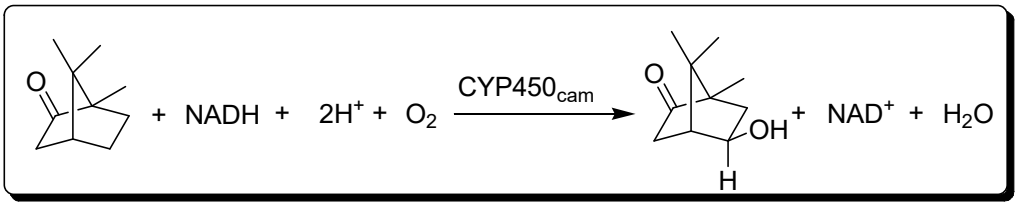

Scheme 3. Stereospecific hydroxylation of the *exo* C-H bond at position 5 of camphor by $CYP450_{cam}$.

Cytochrome P450 enzymes are aptly named as a result of the observation that reduced protein efficiently binds carbon monoxide yielding a complex with a strong absorption at 450 nm.[9] As a result of both the efficiency of cytochrome P450 enzymes to catalyze a variety of difficult biotransformation and its unique spectral properties, creating artificial mimics of these remarkable enzymes has become a logical and intense research focus.[3b, 10] An iron(IV)-oxo porphyrin radial cation, termed as compound I, is widely believed to be the active oxidant in CYP450s enzymes.[11] In this regard, iron, manganese and ruthenium transition metals have been employed as substrate-selective catalysts as biomimetic models of the cytochrome P450 enzymes.[3b, 12] Stimulated by the desire to create the better understanding of the intricate mechanisms of biochemical oxidation using simple biomimetic models, many synthetic metalloporphyrin complexes have been reported as model compounds of heme-containing enzymes and catalysts for a variety of selective oxidation reactions.[13]

1.2 Compound I and compound II species

Key oxidizing intermediates in the catalytic cycles of oxygen activating iron enzymes as well as synthetic oxidation catalysts have been identified as high-valent iron-oxo species.[7, 14] With the intention of gaining a better understanding of the enzymatic reaction mechanisms, synthetic iron porphyrin complexes have been widely used as models of heme-containing enzymes. Various oxidants, such as iodobenzene diacetate,

m-chloroperoxybenzoic acid, iodosobenzene, and ozone, in reaction with iron(III) porphyrin complexes, have been shown to form iron(IV)-oxo porphyrin radial cations (termed as compound I models) and neutral iron(IV)-oxo porphyrin (termed as compound II models) (Scheme 4).[2, 13b]

The fast mixing studies of CYP450s with external oxidants gave only protein radical and ferryl species within 8 ms by the freeze-quench technique.[15] Based on the physical characterization data presently available for the CYP450s oxidant, the compound I state (as well as the peroxo and hydroperoxy states of the enzyme) have been proposed to be the active species in oxygenation events.[16]

It is important to note that the iron(V)-oxo species would be formed directly from heterolytic peroxy bond cleavage after the second protonation on the distal O-H atom. This perferryl iron-oxo transient could serve as either an intermediate or a transition state in the CYP450s oxidation process, depending upon the energy barrier for internal electron transfer (ET). Based upon the calculations of Ghosh and co-workers, the perferryl iron-oxo species should have a higher energy than the corresponding ferryl-oxo porphyrin radical cation. These calculations imply a possible higher reactivity for this species compared to the compound I species.[17]

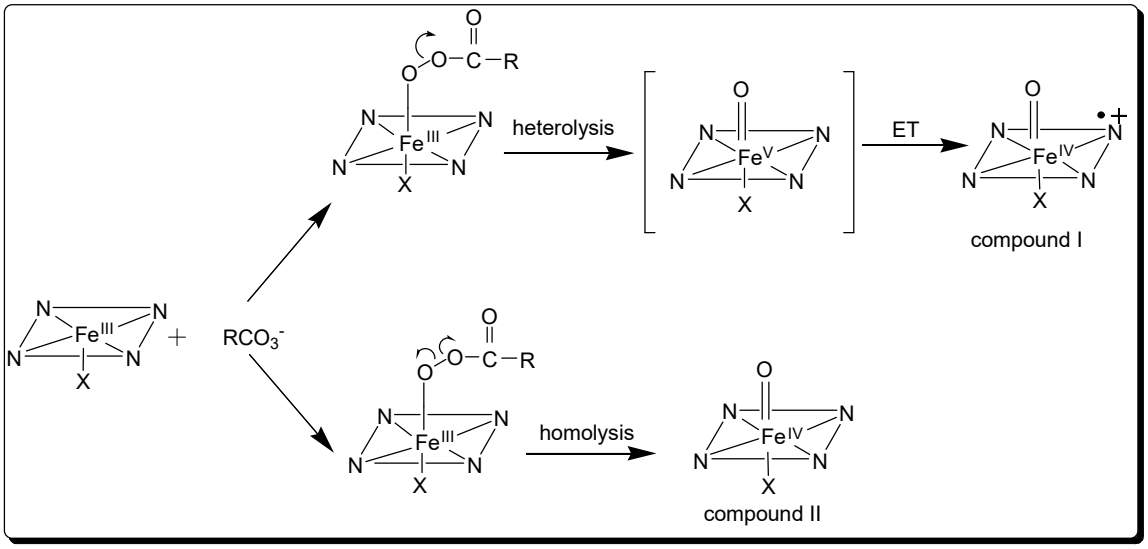

Scheme 4. Chemical generation of compound I and compound II species.

1.3 Biomimetic oxidation by metalloporphyrins

Most biological oxidations involved sophisticated electron and proton transfer steps to activate molecular oxygen, and are difficult to implement in practice.[10] In this regard, metalloporphyrins have been widely used as biomimetic models of CYP450 enzymes in many catalytic oxidations. Many transition metal catalysts, with a core structure closely resembling that of the iron porphyrin core of CYP450 enzymes, have been synthesized as models to invent enzyme-like oxidation catalysts as well as to probe the sophisticated mechanism of molecular oxygen activation.[2] Metalloporphyrin have

been widely used as biomimetic models of cytochrome P450 enzymes to catalyze a variety of oxidation reactions (Scheme 5).

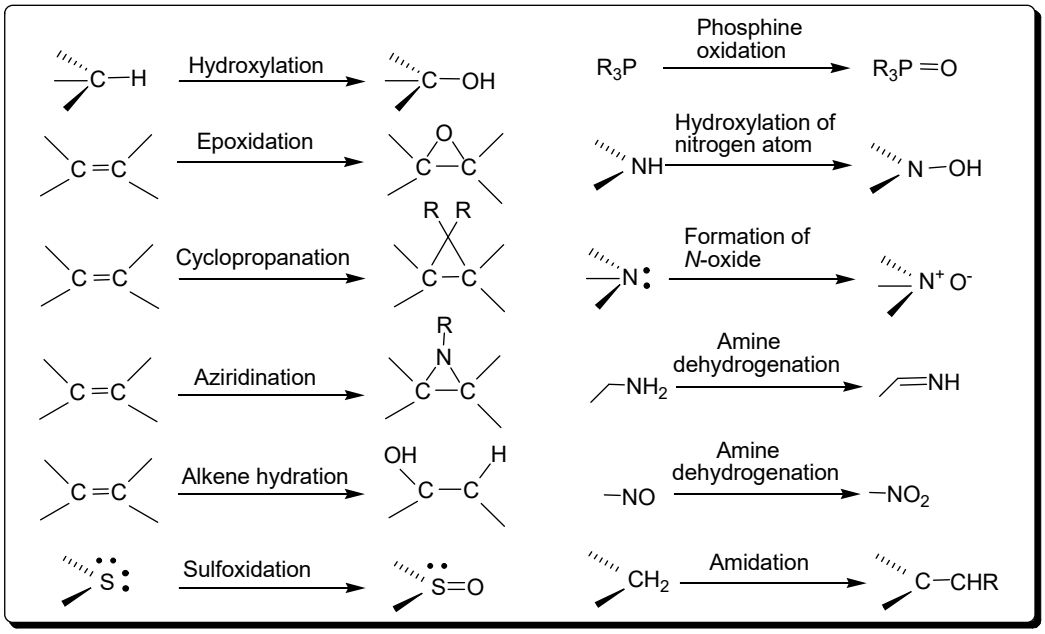

Scheme 5. Typical metalloporphyrin-mediated reactions.

In 1981, Groves and co-workers reported the first synthesis and characterization of a compound I-like model species.[18] The oxidation of ferric porphyrin chloride complex [Fe^{III}(TMP)Cl] (TMP=5,10,15,20-tetramesitylphenylporphyrin) with 1.5 equivalents of *m*-CPBA at room temperature generated a green iron(IV)-oxo porphyrin radical cation species (compound I). This compound I analogue was further characterized with UV-visible, NMR, and EPR spectroscopic methods.[19] It has also been reported that

reaction of the [Fe^{III}(TDCPP)(ClO_4)] with *m*-CPBA in acetonitrile at -35°C gave a compound I species.[20]

In the same report, Groves and co-workers presented the oxidation reaction of the same ferric porphyrin [Fe^{III}(TMP)Cl] by 1 equivalent of PhIO at -78°C in CH_2Cl_2, affording an iron(IV)-oxo neutral species (compound II).[18] Oxidation of[Fe^{III}(TDCPP)OH] with *m*-CPBA also generated porphyrin-iron(IV)-oxo compound II complexes.[21] Another preparation and characterization of compound II species found they are relatively more stable than the iron (IV)-oxo porphyrin radical cation.[21-22] Therefore, compound II species are less reactive in oxo transfer reactions in comparison to compound I species.[7, 23]

In addition, over the past 20 years, considerable attention has been given to high-valent ruthenium-oxo and manganese-oxo porphyrin complexes. In 1997, Groves and his group reported the first manganese(V)-oxo porphyrin intermediates in aqueous solution which show unusually high reactivity in olefin epoxidation and alkanehydroxylation.[13a, 24] Ruthenium porphyrins and related complexes have attracted intense attention, as ruthenium complexes have a variety of useful characteristics including rich coordination, low redox potentials, high electron transfer ability, and stability of reactive metal species.[6] Ruthenium porphyrin complexes have been developed as enzyme-like catalysts for selective oxidation methods.[6]

1.4 Photochemical generation of high-valent metal-oxo species

Photochemistry is of special interest in exploring metal-oxo chemistry[25] as most chemical synthetic methods involve the use of toxic or polluting reagents. Visible light (sunlight) used to induce reversible redox processes of the metal center could avoid all of disadvantages deriving from the use of chemical reagents.[4b] Laser flash photolysis methods have been developed to generate a variety of high-valent transition metal-oxo species supported by porphyrin and corrole ligands.[26] Photochemical production of reactive metal-oxo intermediates also has access to time scales that are much shorter than the fastest mixing experiments.

In addition, a significant difference between photochemical and chemical methods is that the kinetics of the photo-generated intermediates is not convoluted with the rate constants for formation of the reactive transients by reaction of the sacrificial oxidant with the low-valent metal species.[27] To exploit this difference, Newcomb and co-workers have developed photo-induced ligand cleavage reactions for production of high-valent transition metal-oxo derivatives.[28] The mechanism of the photo-induced ligand cleavage reaction is illustrated in Scheme 6. The precursor complexes have metal in the n oxidation state and an oxygen-containing ligand. Photolysis can result in homolytic cleavage of the O-X bond in the ligand to give an (n+1) oxidation state metal-oxo species or heterolytic cleavage in the ligand to give an (n+2) oxidation state metal-oxo species.

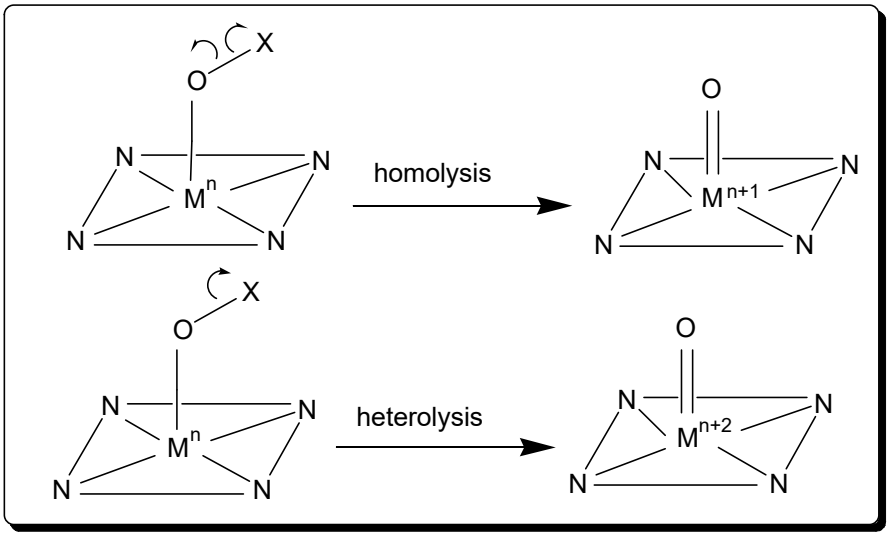

Scheme 6. Photo–induced ligand cleavage reactions for production of high-valent transition metal-oxo species.

This photochemical approach produces metal-oxo species instantly, permitting direct detection of high-valent metal-oxo species and kinetic studies of their oxidations. It is our goal to develop noteworthy new methods of using photochemical ligand cleavage reactions in order to generate active high-valent macrocyclic metal-oxo species. In this study, visible light induced-ligand cleavage reactions have been extended to generate and study high-valent iron(IV)-oxo and manganese(IV)-oxo intermediates supported by two porphyrin ligands.

In Chapter 3, a series of iron(IV)-oxo and manganese(IV)-oxo porphyrin species were synthesized by photochemical and chemical methods. This study focuses on synthetic, spectroscopic and kinetic studies of iron(IV)-oxo porphyrins.

CHAPTER 2

EXPERIMENTAL SECTION

2.1 Materials

All the chemicals in this work were purified and used without further purification unless otherwise specified. All the organic solvents for synthesis and purification were analytical grade, including acetone, acetonitrile, chloroform, dichloromethane, ethanol, ethyl acetate, hexane, methanol and *N, N*-dimethylformamide (DMF). All solvents were purchased from Sigma-Aldrich Chemical Co. HPLC grade acetonitrile (99.93%) was distilled over P_2O_5 prior to use. All reactive substrates for catalytic oxidations and kinetic studies were purified by passing through a dry Al_2O_3 (Grade I, neutral) column before use, including cyclohexene, *cis*-cyclooctene, *cis*-stilbene, ethylbenzene, ethylbenzene-d_{10}, styrene, 4-chlorostyrene, 4-fluorostyrene, 4-methystyrene, 4-methoxystyrene, 1-phenylethanol, diphenylmethane, thioanisole, 4-methoxythioanisole, 4-methylthioanisole, 4-chlorothioanisole, 4-fluorothioanisole, 2,6-dichlorobenzaldehyde, 2,6-difluorobenzaldehyde, boron trifluoride diethyl etherate ($BF_3 \cdot Et_2O$), pyrrole, 2,3-dichloro-5,6-dicyano-p-benequimone (DDQ), manganese(II) acetate tetrahydrate, iron(II) chloride, chloroform-*d*, iodobenzene diacetate [$PhI(OAc)_2$] was obtained from Sigma-Aldrich Chemical Co. and used as such. All bromate and chlorate precursors of the metalloporphyrin complexes were prepared by stirring with an excess of sliver

bromate ($AgBrO_3$) or silver chlorate ($AgClO_3$) with [Fe^{III}(Por)Cl] or [Mn^{III}(Por)Cl]. The resulting solutions were used for photolysis studies immediately after preparation.

2.2 Methods

2.2.1 Physical measurement

^{1}H-NMR was measured using a JEOL ECA-500 MHz spectrometer at 298 K with tetramethylsilane (TMS) as internal standard. Chemical shifts (ppm) were reported relative to TMS. UV-vis spectra were measured using an Agilent 8453 diode array spectrophotometer. Kinetic measurements were performed on the same spectrophotometer by using standard 1.0-cm quartz cuvettes (Figure 3). Visible light was produced from a SOLA SE II light engine (Lumencor) configured with a liquid light guide (6-120W) or from a tungsten lamp (60-300W).

Figure 3. Agilent 8454 diode array UV-vis spectrophotometer (right) and SOLA light engine with the Light (left).

2.2.2 Pyrrole purification

The commercially available pyrrole was purified by distillation. Pyrrole was added into a 50-mL round-bottom flask which contained a magnetic spin vane. The flask was connected to a short-path distillation apparatus from ChemGlass. Since the boiling point of the pyrrole is 129 ^{o}C, all the distillate was collected at this temperature and the distillate below or above that temperature was abandoned. The freshly distilled pyrrole was directly used for the synthesis of the free porphyrin ligand.

2.2.3 General procedure for photolysis of porphyrin iron(III) bromate [Fe^{III}(Por)(BrO_3)] (**4a - 4b**)

Iron(III) porphyrin complexes [Fe^{III}(Por)Cl] (**2a-b**) were mixed and stirred with excess amounts of Ag(BrO_3) in anaerobic acetonitrile, which produced the corresponding bromate salts. The formation of the precursors [Fe^{III}(Por)(BrO_3)] was confirmed by a change of the UV-vis absorption spectrum. (*Caution! Bromate salts of metal complexes are potentially explosive and should be handle with care.*) The resulting solutions of [Fe^{III}(Por)(BrO_3)] were photo-labile and used for photochemical studies immediately after preparation. A solution with a concentration of 1×10^{-5} M was irradiated under visible light (60-300W) at ambient temperature. The high-valent iron-oxo intermediates were completely formed over a 20 - 30 min period as monitored by UV-vis spectroscopy.

2.2.4 General procedure for photolysis of porphyrin manganese(III) chlorates

$[Mn^{III}(Por)(ClO_3)]$ (**5a - 5b**)

Exchange of the axial ligand in $[Mn^{III}(Por)Cl]$ (**3a-b**) with excess of silver chlorate gave the corresponding chlorate complexes $[Mn^{III}(Por)(ClO_3)]$ (**5a-b**). The process of formation of the chlorate complexes was further characterized by the UV-vis spectra. These species (**5a-b**) were highly photo-labile and were used for photochemical studies immediately after preparation. A solution with concentration of 5×10^{-6} M was irradiated under visible light at ambient temperature, and formation of high-valent manganese-oxo intermediates was complete within 8 s as monitored by UV-vis spectroscopy.

2.2.5 Direct kinetic study of high-valent iron-oxo intermediates

Reactions of high-valent metal-oxo species with a large excess of organic substrates were carried out in 2 mL solutions at 23 ± 2 ºC. It is assumed that $[Fe^{IV}(Por)O]$ complexes (**6a-b**) were quantitatively converted from iron(III) bromate precursors (**4a-b**) in the photochemical or chemical reactions. The rates of the reactions were measured by the decay of Soret and Q bands characteristic of the oxo-species, which represent the rates of oxo-transfer from $[Fe^{IV}(Por)O]$ (**6a-b**) to the organic substrates. Kinetics were

measured with single-turnover experiments using excess reductants to achieve pseudo-first-order kinetic conditions. Rate constants for decay reactions were determined by kinetic measurements with varied concentrations of substrates. Kinetic traces at λ_{max} of the Soret band displayed good pseudo-first-order behavior, and the pseudo-first-order observed rate constants (k_{obs}) were obtained after the data was processed. The second-order rate constants for reactions of the oxo species with organic substrates were determined according to Eq. 1, where k_o is a background rate constant found in the absence of organic substrate, k_{ox} is the second-order rate constant for reaction with the substrate, and [Sub] is the concentration of substrate. All second-order rate constants are averages of 2-3 determinations consisting of three independent kinetic measurements. Errors in the rate constants were weighted and are at the 2σ level.

$$k_{obs} = k_o + k_{ox}[\text{Sub}] \quad (1)$$

2.2.6 General procedure for catalytic competition studies

A CH_3CN solution containing equal amounts of two substrates, e.g. thioanisole (0.2 mmol) and substituted thioanisole (0.2 mmol), iron(III) porphyrin catalyst (1 μmol) and 5 μL H_2O was prepared (final volume = 0.7 mL). $PhI(OAc)_2$ (0.1 mmol) was added as the limiting reagent, and the mixture was stirred under an inert atmosphere at ambient temperature until the reaction was complete (Ca. 10 min). Relative rate ratios for catalytic oxidations were determined by GC (FID) based on the amounts of sulfoxide products as measured against an internal standard. With limited $PhI(OAc)_2$ (0.25 equivalent of

substrates), all the catalytic oxidation reactions proceeded with good yields (>99%), mass balance (> 95%), and only traces of sulfones were detected (< 1% by GC). Thus, the ratio of product formation should reasonably reflect the relative sulfide reactivity toward the porphyrin-iron-catalyzed oxidations. The values reported in Table 3 are the averages of 2–3 runs with a minor error (< 5%). Control experiments demonstrated that $PhI(OAc)_2$ gave no detectable amount of sulfoxide product (< 1%) in the absence of iron(III) catalysts.

2.3 Synthesis and characterization

2.3.1 Synthesis of 5,10,15,20-tetrakis(2,6-dichlorophenyl) porphyrin [H_2(TDCPP)] (**1a**) and 5,10,15,20-tetrakis(2,6-difluorophenyl) porphyrin [H_2(TDFPP)] (**1b**)

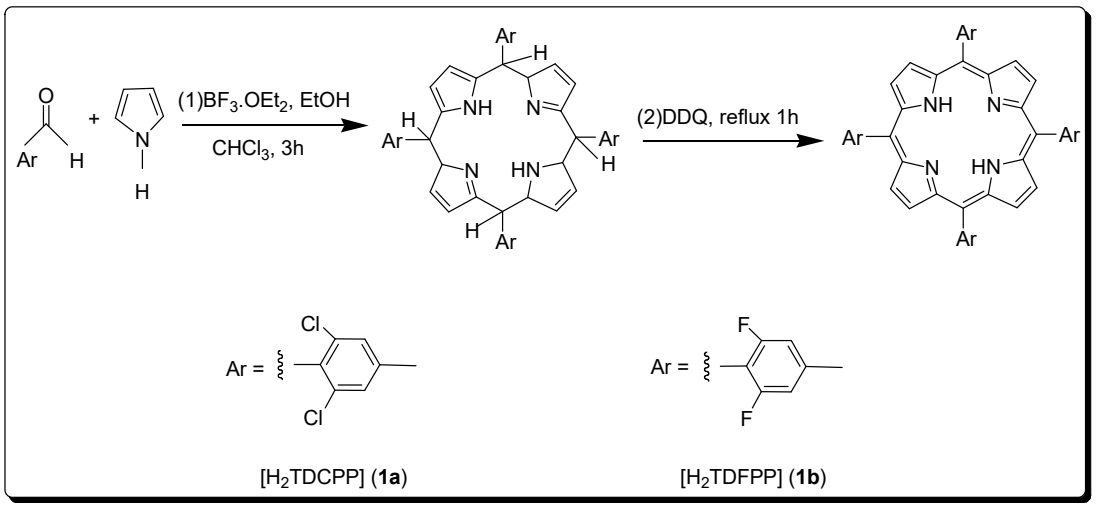

Scheme 7. Two-step synthesis of [H_2(TDCPP)] (**1a**) and [H_2(TDFPP)] (**1b**).

As shown in Scheme 7, the sterically encumbered free porphyrin ligands (**1a-b**) were synthesized according to the known method.[29] Freshly distilled pyrrole (347 µL, 5 mmol), 2,6-dichlorobenzaldehyde (5 mmol, 875 mg) and chloroform (500 mL) were added in a 1 L three-neck round-bottomed flask fitted with a septum and reflux condenser. Ethyl alcohol (3.2 mL, 0.5% v/v) was added as a co-catalyst. The solution was purged with Argon for 5 min. Boron trifluoride diethyl etherate ($BF_3.OEt_2$) (660 µL, 1.65 mmol) was injected into the solution in a dropwise manner, and the reaction mixture was stirred for about 3 h at room temperature. The co-catalyst of $BF_3.OEt_2$ and ethanol generates the Brønsted acid (BF_3-EtOH) which catalyzes the pyrrole-aldehyde condensation to form the porphyrinogen intermediate.

The reaction was monitored by UV-vis spectroscopy to confirm the formation of porphyrinogen intermediate. After stirring, 2,3-dichloro-5,6-dicyano-*p*-benequimone (DDQ) (957 mg) was added into the mixed solution. The mixture was gently refluxed for 1 h, and cooled down to room temperature. Triethylamine (920 µL, 6.6 mmol) was added to neutralize the mixture, and the solution was evaporated to dryness. The crude solid product was washed with a large excess of methanol under vacuum until the filtrate was clear. Further purification was performed by column chromatography (silica gel). After loading the product into the column, dichloromethane was used to elute the desired

product. The [H_2(TDCPP)] (**1a**) was obtained as purple solid and characterized by UV-vis (Figure 4A) and ^{1}H-NMR (Figure 4B). Another sterically hindered system [H_2(TDFPP)] (**1b**), was successfully synthesized using the same procedure and the spectroscopic characterization data were shown in Figure 5A and 5B.

5,10,15,20-tetrakis(2,6-dichlorophenyl) porphyrin [H_2(TDCPP)] (1a)

Yield = 205 mg (24 %)

UV-vis (CH_2Cl_2) λ_{max}/nm: 418 (Soret), 512, 590. (Figure 4A)

^{1}H-NMR (500 MHz, $CDCl_3$): δ, ppm: -2.70 (s, 2H, NH), 7.75 (m, 12H, m-Ar-H and P-Ar-H), 8.83 (s, 8H, β-pyrrolic-H). (Figure 4B)

5,10,15,20-tetrakis(2,6-difluorophenyl) porphyrin [H_2(TDFPP)] (1b)

Yield = 203 mg (20.5 %)

UV-vis (CH_2Cl_2) λ_{max}/nm: 411 (Soret), 507, 580. (Figure 5A)

^{1}H-NMR (500 MHz, $CDCl_3$): δ, ppm: -2.78 (s, 2H, NH), 7.78 (m, 12H, m-Ar-H and P-Ar-H), 8.87 (s, 8H, β-pyrrolic-H). (Figure 5B)

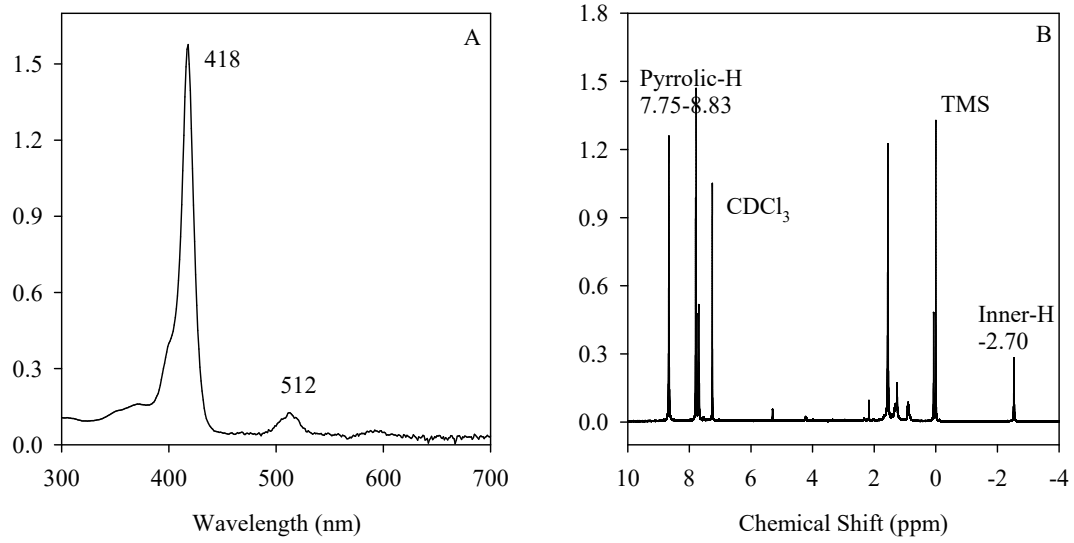

Figure 4. (A) The UV-vis spectrum of [H_2(TDCPP)] (**1a**) in CH_2Cl_2; (B) The ^{1}H-NMR spectrum of [H_2(TDCPP)] (**1a**) in $CDCl_3$.

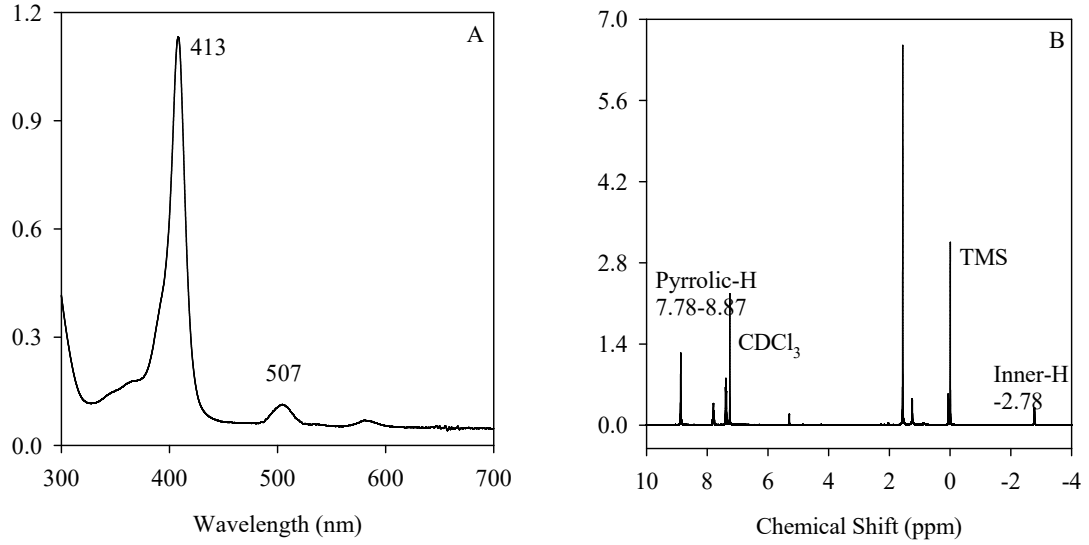

Figure 5. (A) The UV-vis spectrum of [H_2(TDFPP)] (**1b**) in CH_2Cl_2; (B) The ^{1}H-NMR spectrum of [H_2(TDFPP)] (**1b**) in $CDCl_3$.

2.3.2 Synthesis of iron(III) porphyrin chloride [Fe^{III}(Por)Cl] and manganese(III) porphyrin chloride [Mn^{III}(Por)Cl]

Iron(III) and manganese(III) porphyrin complexes (**2** and **3**) were prepared by metalation of the free porphyrin ligand [H_2(TDCPP)] (**1a**) or [H_2(TDFPP)] (**1b**) with $FeCl_2$ or $Mn(OAc)_2$ in dimethylformamide (DMF) as described in Scheme 8 and 9.[30] Fe^{III} and Mn^{III} species were characterized by UV-vis and ^{1}HNMR, matching those reported.

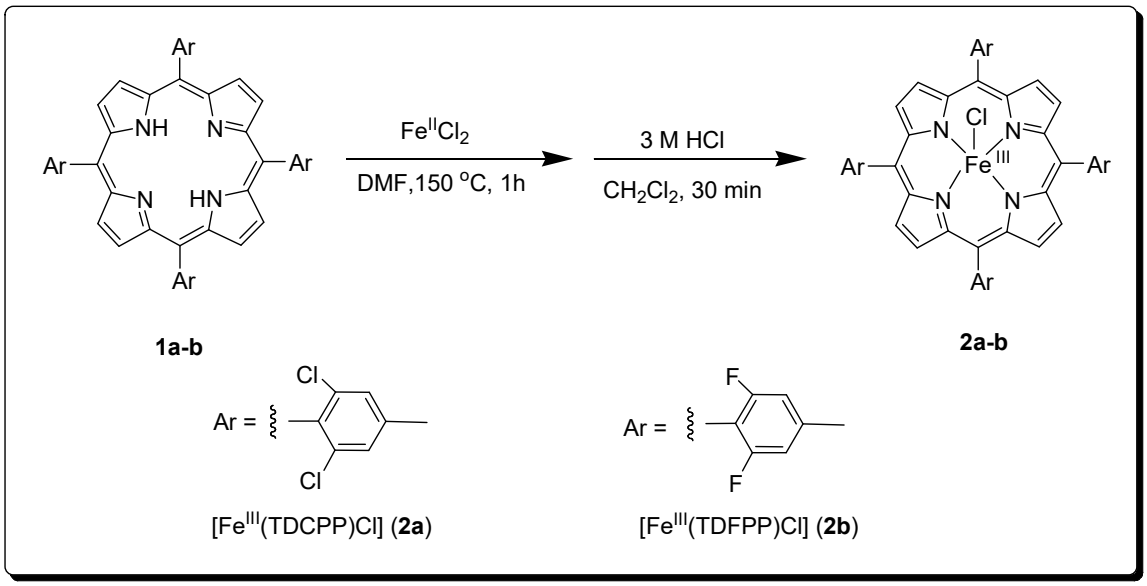

Scheme 8. Synthesis of [Fe^{III}(Por)Cl] (**2a-b**).

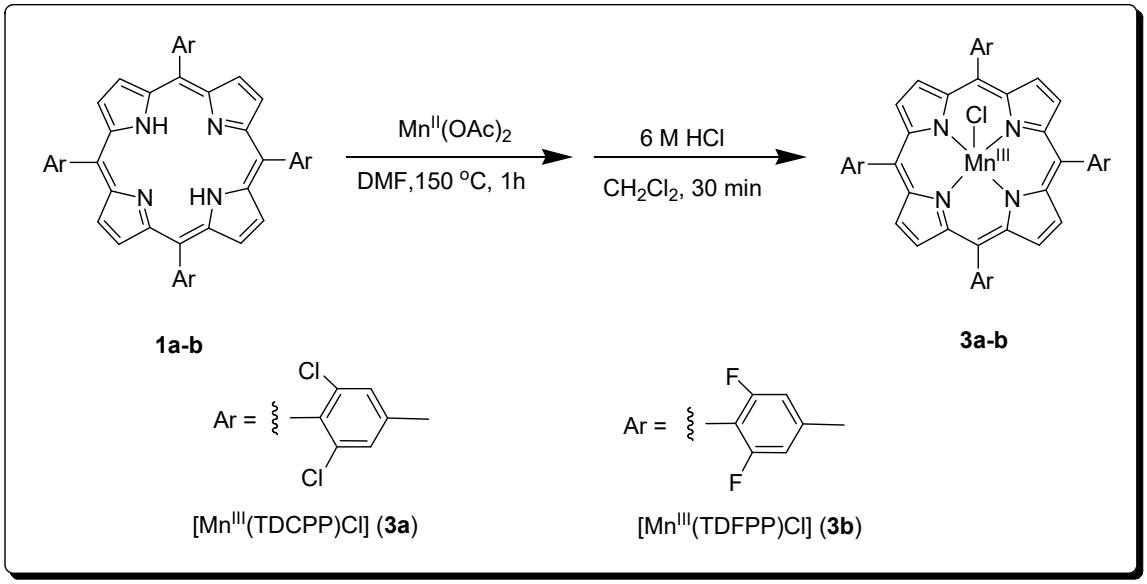

Scheme 9. Synthesis of [Mn^{III}(Por)Cl] (**3a-b**).

Following the typical procedure,[30] porphyrin free ligand (**1a** or **1b**) (100 mg) was dissolved in DMF(30 mL) in a two-neck round-bottom flask fitted with reflux condenser. The solution was degassed with argon for 5 min. A large excess of manganese(II) acetate tetrahydrate (300 mg) or iron(II) chloride (500 mg) was added. The mixture was heated gently and refluxed for 30-60 min. UV-vis spectroscopy and TLC analysis were used to monitor the reaction process. The DMF solvent was evaporated to dryness under vacuum. The crude product was collected and dissolved in CH_2Cl_2. HCl (3 M 50 mL) was added and the resulting solution was stirred for 30 min. The original axial ligand was substituted by Cl^- in this process. The solution was extracted with dichloromethane and washed with distilled water. Na_2SO_4 was then added to remove any remaining water. The product was

further purified by column chromatography (silica gel) using CH_2Cl_2 as eluent. The desired metalloporphyrin complexes [Fe^{III}(Por)Cl] (**2a**-**b**) and [Mn^{III}(Por)Cl] (**3a**-**b**) were characterized by UV-vis and ^{1}H-NMR (Figures 6-9).

Iron(III) 5, 10, 15, 20-tetrakis(2,6-dichlorophenyl) porphyrin chloride

[Fe^{III}(TDCPP)Cl] (2a) Yield = 70 mg (70%).

UV-vis (CH_2Cl_2) λ_{max}/nm: 414 (Soret), 381, 510. (Figure 6A)

^{1}H-NMR (500MHz, $CDCl_3$): δ, ppm: 82.3 (s, 8H, β-pyrrolic-H). (Figure 6B)

Iron(III) 5, 10, 15, 20-tetrakis(2,6-difluorophenyl) porphyrin chloride

[Fe^{III}(TDFPP)Cl] (2b) (Figure 8) Yield = 82 mg (82 %).

UV-vis (CH_2Cl_2) λ_{max}/nm: 411 (Soret), 366, 508. (Figure 7A)

^{1}H-NMR (500MHz, $CDCl_3$): δ, ppm: 82.6 (s, 8H, β-pyrrolic-H). (Figure 7B)

Manganese(III) 5, 10, 15, 20-tetrakis(2,6-dichlorophenyl) porphyrin chloride

[Mn^{III}(TDCPP)Cl] (3a)

Yield = 88 mg (88 %).

UV-vis (CH_2Cl_2) λ_{max}/nm: 476 (Soret), 371, 581. （Figure 8A)

^{1}H-NMR (500MHz, CDCl3): δ, ppm: -21.1 (s, 8H, β-pyrrolic-H). (Figure 8B)

Manganese(III) 5, 10, 15, 20-tetrakis(2,6-dichlorophenyl) porphyrin chloride

[Mn^{III}(TDFPP)Cl] (3b) Yield = 80mg (80%).

UV-vis (CH_2Cl_2) λ_{max}/nm: 472 (Soret), 368, 570, 628. (Figure 9A)

^{1}H-NMR (500MHz, CDCl3): δ, ppm: -22.0 (s, 8H, β-pyrrolic-H). (Figure 9B)

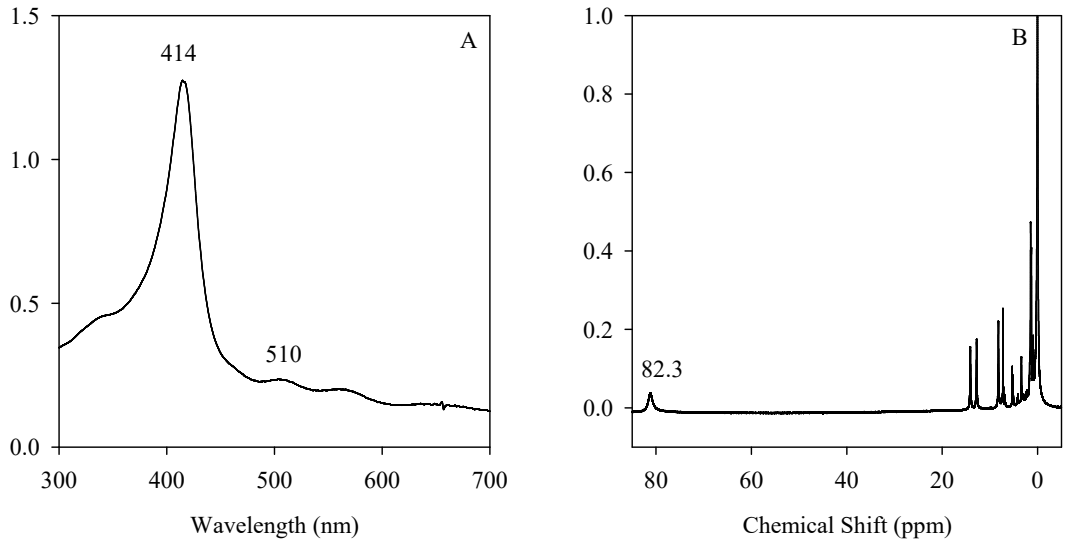

Figure 6. (A) The UV-vis spectrum of [Fe^{III}(TDCPP)Cl] (**2a**) in CH_2Cl_2; (B) The ^{1}H-NMR spectrum of [Fe^{III}(TDCPP)Cl] (**2a**) in $CDCl_3$.

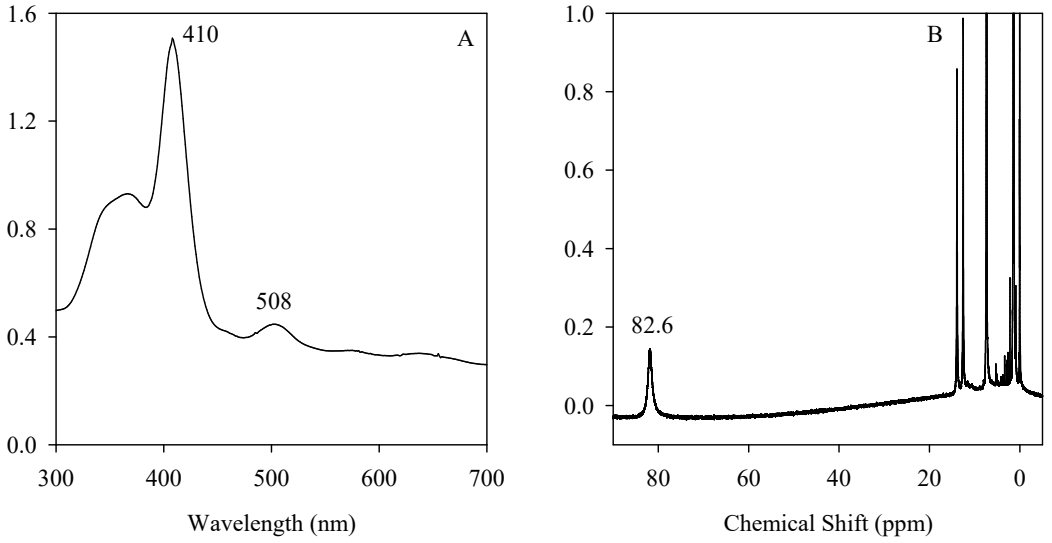

Figure 7. (A) The UV-vis spectrum of [Fe^{III}(TDFPP)Cl] (**2b**) in CH_2Cl_2; (B) NMR spectrum of [Fe^{III}(TDFPP)Cl] (**2b**) in $CDCl_3$.

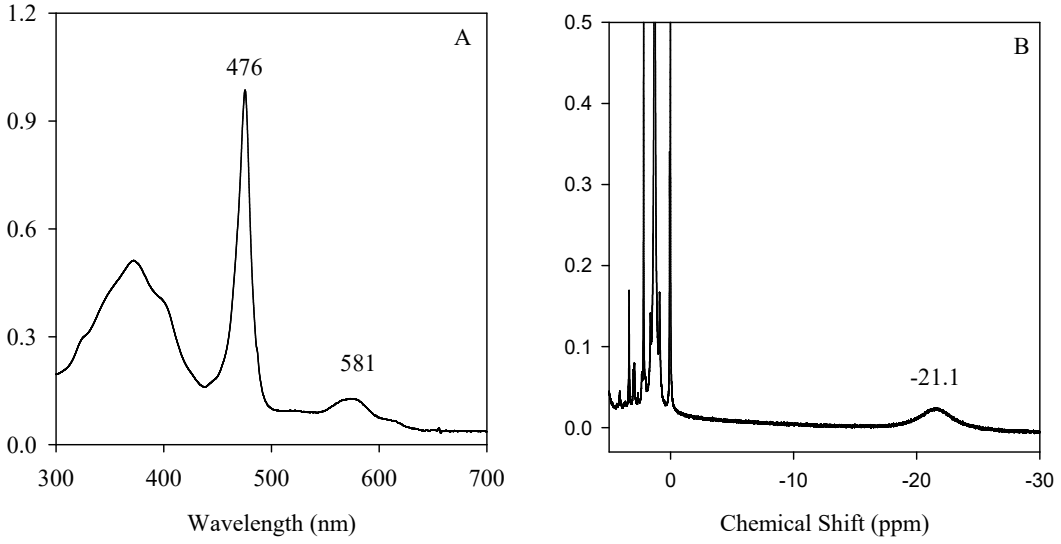

Figure 8. (A) The UV-vis spectrum of [Mn^{III}(TDCPP)Cl] (**3a**) in CH_2Cl_2; (B) The ^{1}H-NMR spectrum of [Mn^{III}(TDCPP)Cl] (**3a)** in $CDCl_3$.

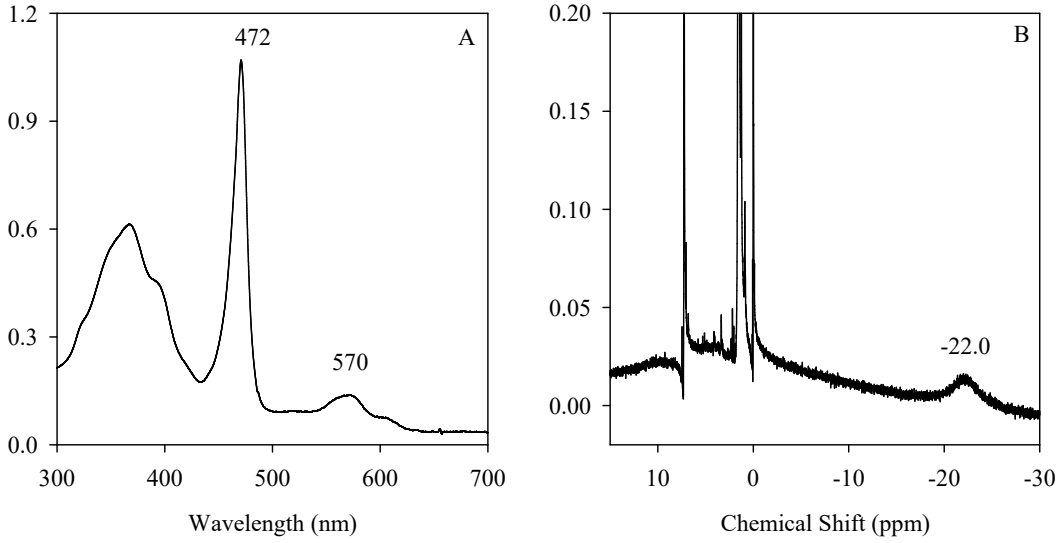

Figure 9. (A) The UV-vis spectrum of [Mn^{III}(TDFPP)Cl] (**3b**) in CH_2Cl_2; (B) The ^{1}H-NMR spectrum of [Mn^{III}(TDFPP)Cl] (**3b**) in $CDCl_3$.

CHAPTER 3

IRON(IV)-OXO AND MANGANESE(IV)-OXO PORPHYRIN SPECIES GENERATED BY PHOTOCHEMICAL AND CHEMICAL METHODS

3.1 Introduction

In enzymatic and synthetic oxidations, high-valent transition metal-oxo species have often been identified as the oxygen atom transfer (OAT) agents.[13a] In this regard, metal-oxo complexes have received considerable attention because of their synthetic utility in various oxidation reactions and relevance to a variety of oxidative enzymes in Nature.[7, 14c, 31] In this chapter, porphyrin-iron(IV)-oxo complexes (**6a**-**b**) (compound II models) and porphyrin-manganese(IV)-oxo species (**7a**-**b**) were produced and studied by photochemical and chemical methods. With iodobenzene diacetate [$PhI(OAc)_2$] as the oxygen source, iron(III) and manganese(III) porphyrin complexes converted to the corresponding metal(IV)-oxo species which function as OAT agents. As an alternative to chemical oxidation, a new photochemical method was developed to generate the same oxo species. In the two electron-deficient systems, iron(IV)-oxo porphyrin derivatives (**6a**-**b**) were produced by visible light irradiation of the corresponding iron(III) bromate complexes. In a similar fashion manganese(IV)-oxo porphyrin (**7a**-**b**) were obtained by photolysis of corresponding manganese(III) chlorate precursors.

3.2 Generation of porphyrin-iron(IV)-oxo species

3.2.1 Chemical generation of porphyrin-iron(IV)-oxo complexes

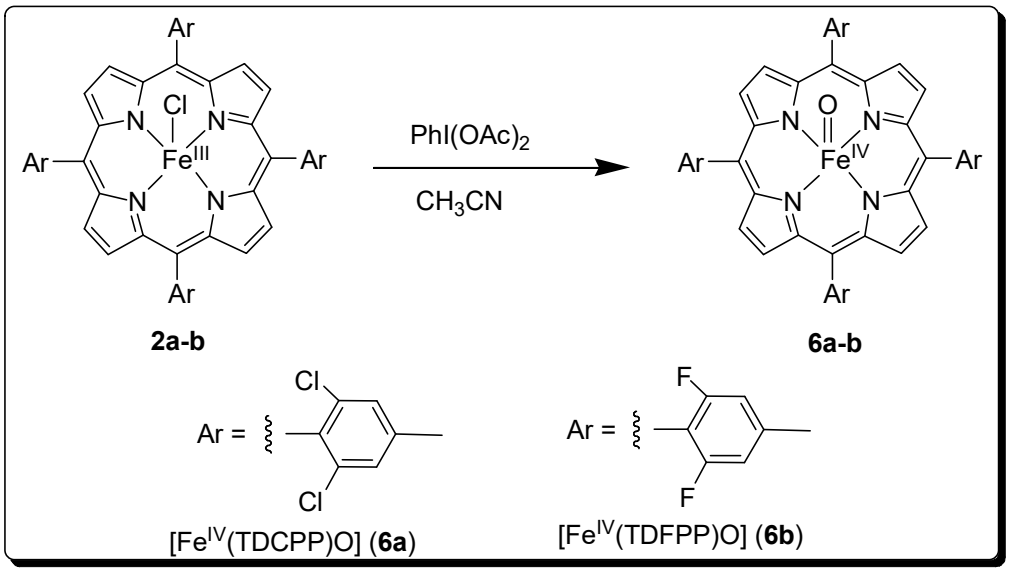

Scheme 10. Chemical generation of iron(IV)-oxo species (**6a-b**).

The chemical-generated systems[32] studied in this chapter are shown in Scheme 10. Ferric porphyrin chloride complexes (**2a-b)** (10 μM) with excess $PhI(OAc)_2$ in 2 mL acetonitrile solution gave the iron(IV)-oxo complexes (**6a-b)**, The process was indicated qualitatively by a color change from light red to dark red. The UV-vis spectra of each iron(IV)-oxo complexes (**6a-b**) (Figure 10A and B) displayed Soret bands that were sharper, more intense and red-shifted from the iron(III) species, and the Q-bands were distinct, indicating a transformation from ferric chloride (**2a-b)** to ferryl-oxo complexes

(**6a-b**). Figure 10A shows the time -resolved spectra in which [Fe^{III}(TDCPP)Cl] (**2a**) was oxidized to an iron(IV)-oxo species (**6a)** over a 20-min period. The peaks at λ = 417 and 560 nm were identical to the [Fe^{IV}(TDCPP)O] (**6a**). The chloride complex **2a** was fully converted to species **6a** with approximately 5 equiv. of $PhI(OAc)_2$. In dilute solutions, complex **6a** was stable for hours at ambient temperature. A similar time-resolved spectrum for formation of [Fe^{IV}(TDFPP)O] (**6b**) is shown in Figure 10B.

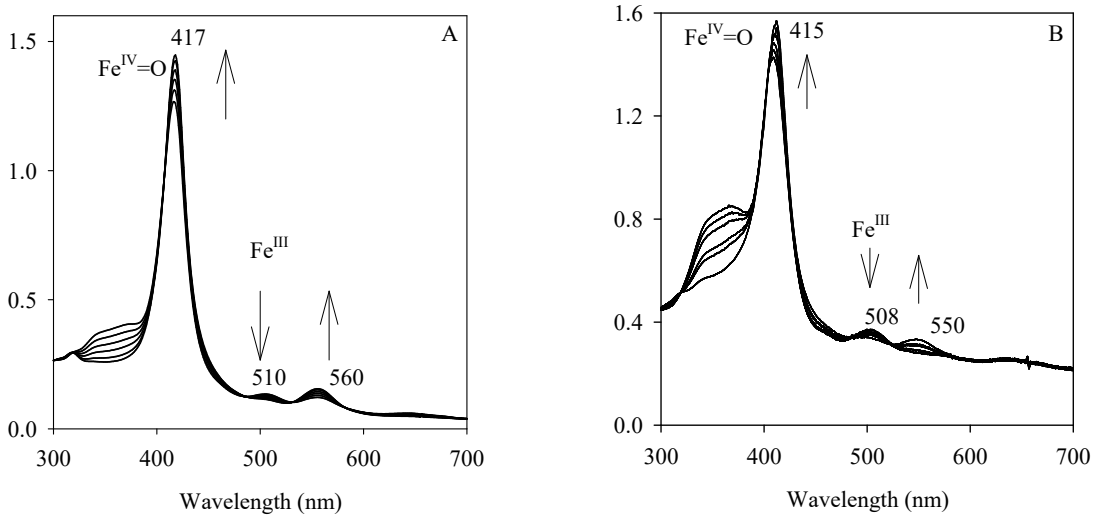

Figure 10. (A) Time-resolved spectra for formation of [Fe^{IV}(TDCPP)O] (**6a**) by oxidation of [Fe^{III}(TDCPP)Cl] (**2a**) with 5 equiv. of $PhI(OAc)_2$ in CH_3CN; (B) Time-resolved spectra for formation of [Fe^{IV}(TDFPP)O] (**6b**) by oxidation of [Fe^{III}(TDFPP)Cl] (**2b**) with 5 equiv. of $PhI(OAc)_2$ in CH_3CN.

3.2.2 Photochemical generation of iron(IV)-oxo porphyrins

In addition to chemical oxidation of iron(III) porphyrins, the photo-induced ligand cleavage reactions have been successfully developed to generate the same iron(IV)-oxo species.[33] Visible light irradiation of bromate complexes (**4a-b)** [Fe^{IV}(Por)(BrO_3)] in anaerobic CH_3CN gave compound II models (**6a-b**) for two electron-deficient porphyrin systems.[33a]

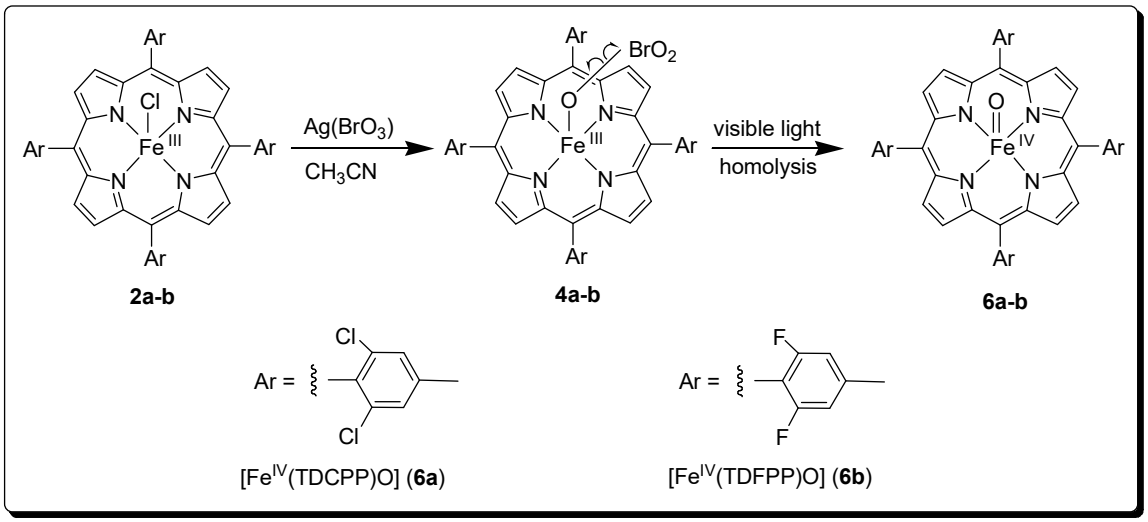

Scheme 11. Photochemical formation of porphyrin-iron(IV)-oxo complexes (**6a-b**)

Iron(III) porphyrin bromate precursors (**4a-b**) were prepared as shown in Scheme 11. Facile exchange of the porphyrin complexes [Fe^{III}(Por)Cl] (**2a-b**) with excess $Ag(BrO)_3$ in anaerobic CH_3CN gave the corresponding bromate salts (**4a-b**), which were

photo-labile and immediately used for photochemical reactions. The solution of **2a** with a concentration of 1.0×10^{-5} M was irradiated with visible light from a SOLA engine (output power 120W) at ambient temperature. The formation of iron(IV)-oxo compound II (**6a**) was complete in a period of 20 to 30 min, as monitored by UV-vis spectroscopy (Figure 11A). The photo transformation is characterized by a distinct color change from brown to red, accompanied by the well-anchored isosbestic points. In each case, the resulting species **6a** display a sharper, stronger, red-shifted Soret and a weaker blue-shifted Q bands, with λ_{max} peak at approximately 417 and 565 nm, that were identical to the corresponding porphyrin-iron(IV)-oxo derivatives. Another electron-deficient system $[Fe^{III}(TDFPP)(BrO_3)]$ (**4b**) was used with the same reaction scheme to generate $[Fe^{IV}(TDFTPP)(O)]$ (**6b**) (Figure 11B).

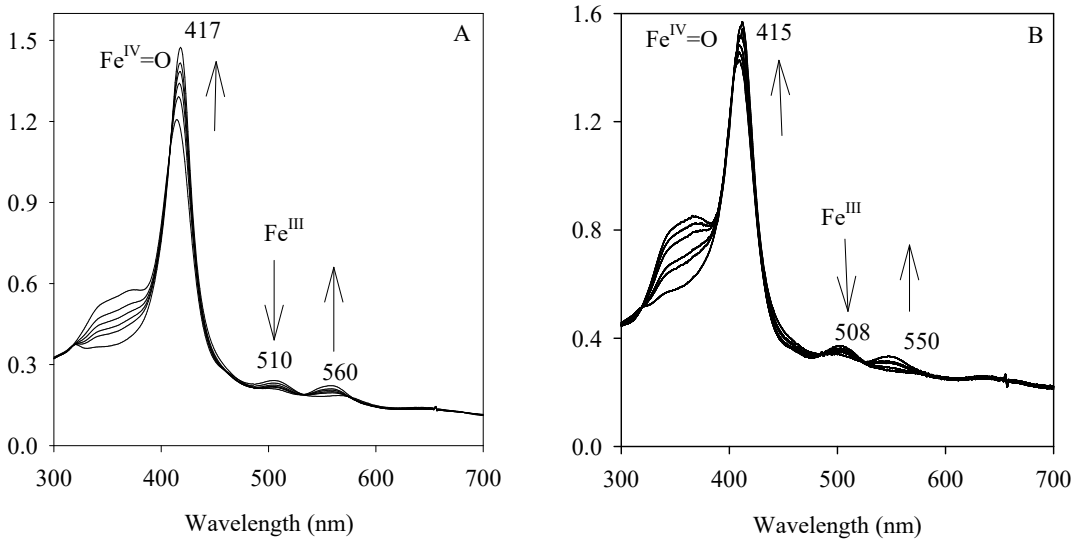

Figure 11. (A) Time-resolved spectra of [Fe^{IV}(TDCPP)O] (**6a**) following irradiation of **2a** with visible light (120 W) in anaerobic CH_3CN solution at 23 ± 2°C over 20 min; (B) Time-resolved spectra of [Fe^{IV}(TDFPP)O] (**6b**) following irradiation of **2b** with visible light (120 W) in anaerobic CH_3CN solution at 23 ± 2°C over 25 min.

Control experiments showed that no oxo species **6** were formed in the absence of light. Photo-generated compound II complexes (**6a-b**) are relatively stable[23b, c] and can be isolated for further characterization, their identities were further confirmed by ^{1}H-NMR spectra.[32a] The same oxo species **6** were produced by chemical and photochemical methods, exhibiting the same spectral signature characteristic for iron(IV)-oxo porphyrins . The observed photochemical formation of **6** can be easily rationalized by a homolytic cleavage of O-Br bond in the counterions of precursor **4**.

As observed in our group's previous studies,[33a] porphyrin-iron(III) bromates which contain non-electron deficient porphyrin ligands, gave porphyrin-iron(IV)-oxo radical cations (compound I models) upon photolysis by a two-electron photo-oxidation of the metal. In contrast, the porphyrin–iron(III) bromates with electron-deficient and sterically encumbered ligands produced iron(IV)-oxo porphyrins via a one-electron photo-oxidation of the metal. The formation of any iron(III) porphyrin radical cations from compound II transients was not observed, suggesting that the internal electron-transfer of ligand to metal ion is not favored in these electron-deficient systems. Thus, the alternative pathway can be ascribed to a two-electron photo oxidation of iron(III) precursors by heterolytic cleavages of O-Br bonds in the counterions of **4,** which initially form a putative iron(V)-oxo intermediate. Apparently, the higher-energy iron(V)-oxo species could quickly reduce to iron(IV)-oxo products by reacting with solvent CH_3CN. Detection and spectroscopic characterization of any initially formed intermediates at low temperature may provide more mechanistic insights into these photochemical processes.

3.3 Generation of porphyrin-manganese(IV)-oxo species

3.3.1 Chemical generation of porphyrin-manganese(IV)-oxo species

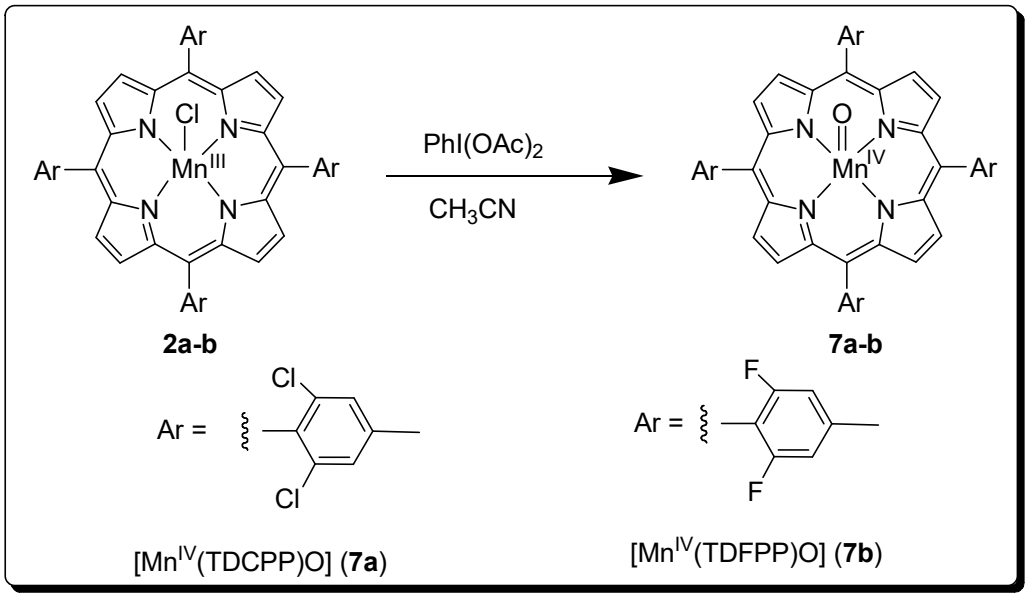

Scheme 12. Chemical generation of manganese(IV)-oxo species (**7a-b**).

The chemical-generated process of porphyrin-manganese (IV)-oxo intermediate formation is shown in Scheme 12. Manganese(III) porphyrin chloride complexes (**3a-b)** (10 μM) with excess $PhI(OAc)_2$ in 2 mL acetonitrile solution gave the manganese(IV)-oxo complexes (**7a-b)**. UV-vis spectra of each complexes (**7a-b)** displayed the Soret band red-shifted from the manganese(III) species, with isosbestic points indicating a clean transformation of manganese(III) chloride (**3)** to the manganese(IV)-oxo complexes (**7**). Figure 12A shows the time-resolved spectra of **3a** as

it is oxidized to **7a** over 6 min. The peaks at λ = 427 and 560 nm are identical to reported data for [Mn^{IV}(TDCPP)O] (**7a**). The chloride complex (**3a**) was fully converted to species **7a** with approximately 30 equivalents of $PhI(OAc)_2$. Time-resolved spectra of [Mn^{IV}(TDFPP)O] (**7b**) are shown in Figure 12B, in which Mn^{III} species reacted with 30 equivalents $PhI(OAc)_2$ and fully converted to Mn^{IV}-oxo **7b**. Complexes (**7a-b)** aren't stable at ambient temperature and decayed back to the Mn^{III} precursors within 8 s.

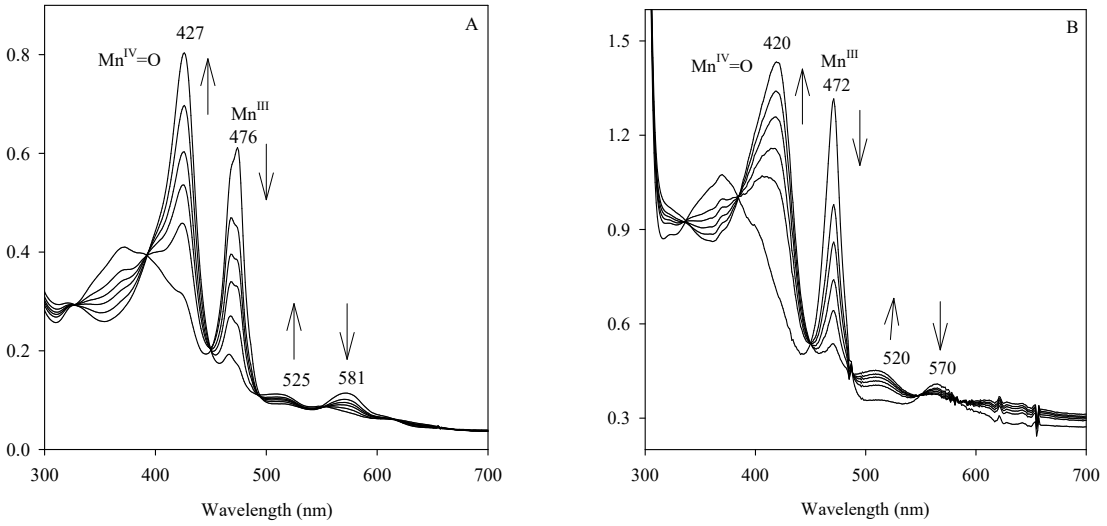

Figure 12. (A) Time-resolved spectra of forming [Mn^{IV}(TDCPP)O] (**7a**) by reacting [Mn^{III}(TDCPP)Cl] (**3a**) with 30 equiv. of $PhI(OAc)_2$ in CH_3CN; (B) Time-resolved spectra of forming [Mn^{IV}(TDFPP)O] (**7b**) by reacting [Mn^{III}(TDFPP)Cl] (**3b**) with 30 equiv. of $PhI(OAc)_2$ in CH_3CN.

3.3.2 Photochemical generation of porphyrin-manganese(IV)-oxo species

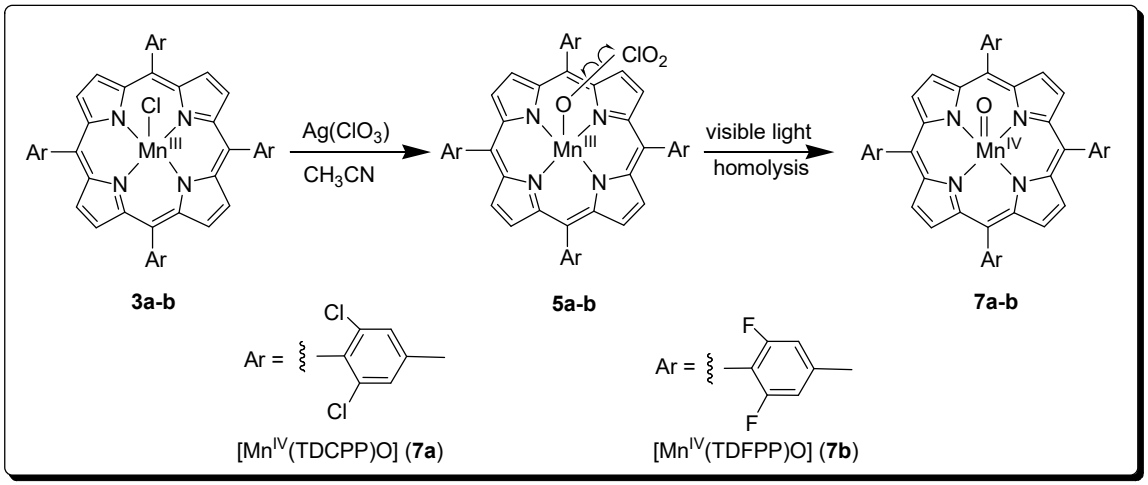

Scheme 13. Photochemical formation of porphyrin-manganese(IV)-oxo complexes by visible light irradiation of manganese chlorate precursors.

The same manganese(IV)-porphyrin-oxo (**7a-b**) produced by photochemical methods[58] were comparatively studied in this chapter. Facile exchange of the counterions in [Mn^{III}(Por)Cl] (**3a-b**) with excess of $AgClO_3$ gave the corresponding chlorate salts (**5a-b**) (Scheme 13 and Figure 13A and 13B), their formations were detected by use of a UV-vis spectrometer.

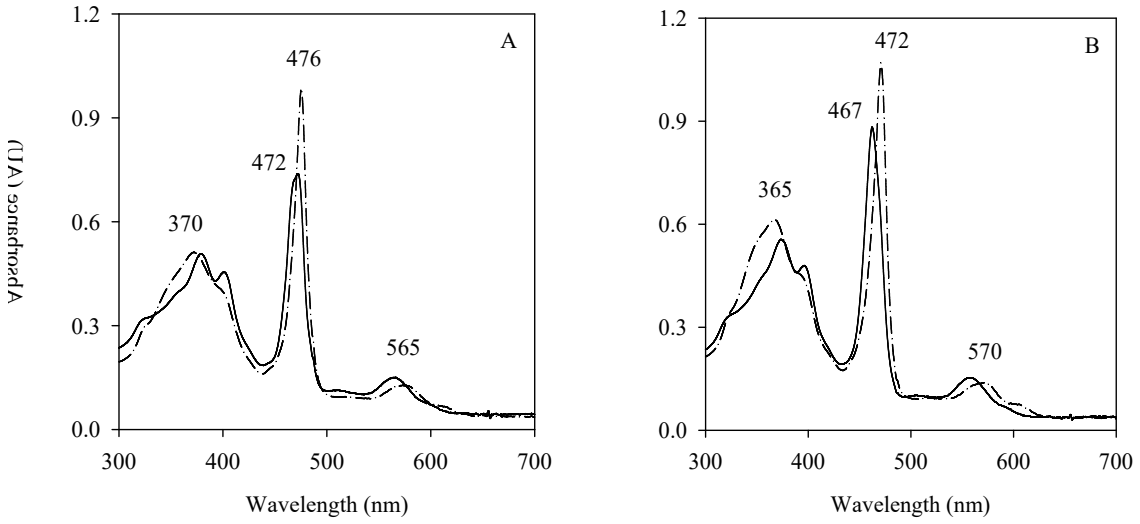

Figure 13. (A) Axial ligand exchange of [Mn^{III}(TDCPP)Cl] (**3a**) with $AgClO_3$ monitored by UV-vis spectroscopy: [Mn^{III}(TDCPP)Cl] (**3a**) (dashed) and [Mn^{III}(TDCPP)ClO_3] (**5a**) (solid); (B) Axial ligand exchange of [Mn^{III}(TDFPP)Cl] (**3b**) with $AgClO_3$ monitored by UV-vis spectroscopy: [Mn^{III}(TDFPP)Cl] (dashed) and [Mn^{III}(TDFPP)ClO_3] (**5b**) (solid).

Like the photochemical cleavage of porphyrin-iron(III) bromates, which give neutral porphyrin-iron(IV)-oxo derivatives by homolytic cleavage of the O-Br bonds in the bromates, photolysis of chlorate complexes (**5a**-**b**) with visible light from a SOLA engine (120W) resulted in homolytic cleavage of an O-Cl bond to give [Mn^{IV}(Por)(O)] derivatives (**7a**-**b**) (Scheme 13), that were characterized by their UV-vis spectra. Figure 14A shows a representative time-resolved formation of spectra of [Mn^{IV}(TDCPP)O] (**7a)** in CH_3CN over 8 s. The peaks at λ = 427 nm and 565 nm were identical to those reported

for [Mn^{IV}(TDCPP)O]. In a same procedure, [Mn^{IV}(TDFPP)(O)] (**7b**) was also generated as shown in Figure 14B.

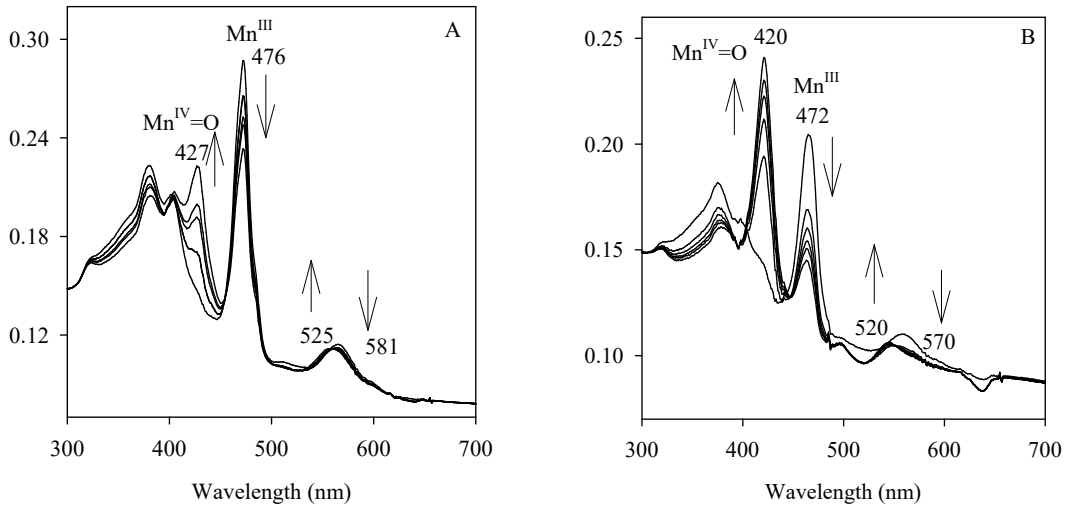

Figure 14. (A) Time-resolved spectra for formation of photo-generated [Mn^{IV}(TDCPP)O] (**7a**); (B) Time-resolved spectra for formation of photo-generated [Mn^{IV}(TDFPP)O] (**7b**).

In this chapter, porphyrin-iron(IV)-oxo and porphyrin-manganese(IV)-oxo complexes in two electron-deficient systems were successfully synthesized by photochemical and chemical methods. Of note, a new photochemical approach provides an additional path to produce iron(IV)-oxo and manganese(IV)-oxo species, which permit direct detection and kinetic studies of catalytic oxidation. In dilute concentration (10 μM), compound II **6** are stable for hours at ambient temperature. On the contrary, Mn(IV)-oxo **7** are much less stable and decayed back to the Mn^{III} precursors.

CHAPTER 4

KINETIC STUIES OF IRON(IV)-OXO COMPOUND II SPECIES

4.1 Introduction

Studies of the kinetics of oxidation reactions of porphyrin-iron(IV)-oxo complexes generated by two methods with organic substrates are described in this chapter. According to recent experimental reports, most of mechanistic investigations of oxygen atom transfer (OAT) reactions by high valent iron-oxo complexes focused on alkene epoxidation and activate alkane hydroxylation in compound I systems.[34] However, kinetic studies of the reactivity of compound II models are rather limited,[23b, 32a] particularly the oxidation of aryl sulfides by iron(IV)-oxo compound II models. In this chapter, we describe kinetic studies of oxidation of alkene, active hydrocarbon and a series of aryl sulfides by compound II models generated by photochemical and chemical methods. We reported rate constants for the OAT reactions of two porphyrin-iron(IV)-oxo compound II models with different organic substrates in acetonitrile solution. A fundamental data set for the kinetics of reactions of P450 compound II models was established. The absolute rate constants for hydroxylation, epoxidation and sulfoxidations by chemical and photochemical generated compound II models in two systems were compared. The comprehensive kinetic data provide mechanistic insights into the identities and reactivities of the active oxidant in the catalytic oxidations.

4.2 Kinetic studies of epoxidation and hydroxylation by iron(IV)-oxo (**6a-b**) generated by photochemical and chemical methods.

It is known that the compound II models **6** act as oxo-transfer agents toward various organic reductants such as alkenes and activated alkenes. Thus, oxidation kinetics of compound II (**6a-b**) generated by two methods with several alkenes and active hydrocarbons were measured. In kinetic studies, 2 mL solutions containing the oxo **6** were mixed with excesses of the organic substrates, and the pseudo-first order rate constants for decay of the compound II species were measured spectroscopically. As reported early, the stabilities of porphyrin-iron(IV)-oxo species were dependent on their concentration.[32a] To avoid uncertainties as result of this concentration effect, we prepared oxo **6** in a similar concentration of approximate 10 μM for all kinetic studies.

The photo-generated [Fe^{IV}(TDCPP)O] (**6a**) decayed in the presence of the organic substrates. The representative time-resolved spectra for reaction of **6a** with substrate is shown in Figure 15A. In the presence of *cis*-stilbene (0.07 M), the oxo **6a** was completely converted into the iron(III) product with hydroxide as the axial ligand.[35] The absorbance in the Soret band region was monitored at 417 nm, which decreased over the process of the reaction. The formation rates for the ferric porphyrin products were measured at λ_{max} = 565 nm for the Q-band signals, and second-order rate constants were determined by Eq.1 as described in the experimental section. Figure 15B shows the decay reaction for chemical-generated **6a** with same concentrations of *cis*-stilbene. The similar

time-resolved spectra for reaction of the photo- and the chemical-generated [Fe^{IV}(TDFPP)O] with *cis*-cyclooctene (0.4 M) are shown in Figure 16A and 16B.

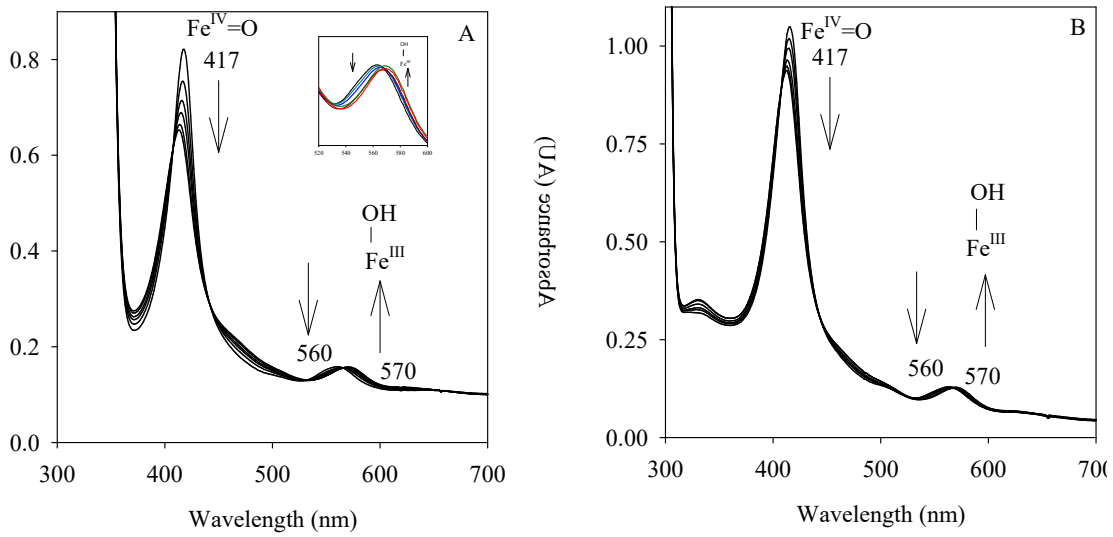

Figure 15. (A) Time-resolved spectra of the oxidation reaction of photo-generated [Fe^{IV}(TDCPP)O] (**6a**) with *cis*-stilbene (70 mM) over 650 s; (B) Time-resolved spectra of the oxidation reaction of chemical-generated [Fe^{IV}(TDCPP)O] (**6a**) with *cis*-stilbene (70 mM) over 800 s.

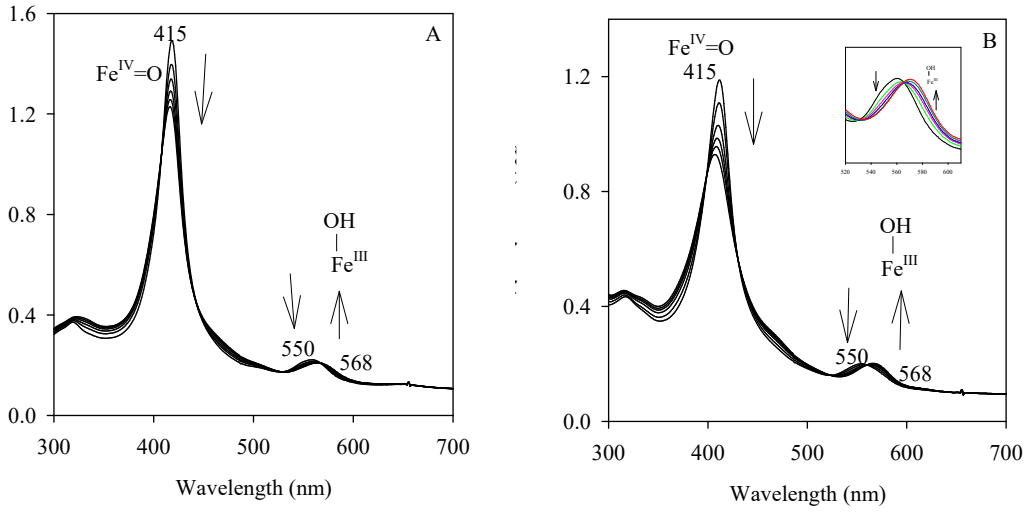

Figure 16. (A) Time-resolved spectra for the reaction of photo-generated [Fe^{IV}(TDFPP)O] (**6b**) with *cis*-cyclooctene (0.4 M) over 400 s; (B) Time-resolved spectra for the reaction of chemical-generated [Fe^{IV}(TDFPP)O] (**6b**) with *cis*-cyclooctene (0.4 M) over 600 s.

The kinetic plots of k_{obs} versus concentration of substrate typically gave straight lines with near-zero intercepts, examples are shown in Figure 18A and 18B. The kinetic plots from reactions of photo-generated **6a** with *cis*-stilbene (0.07 M, 0.14 M, 0.21 M, 0.28 M), 4-methylstyrene (0.15 M, 0.18M, 0.22 M, 0.3 M), diphenylmethane (0.03 M, 0.06 M, 0.075 M, 0.09 M) are shown graphically in Figure 17A, chemical-generated **6a** react with the same three organic substrates are shown in Figure 17B, where plots of k_{obs} versus the concentration of the three substrates are observed to increase linearly. Apparent second-order rate constants for the reaction of **6a** and **6b** generated by the two methods with organic substrates are listed in Table 1.

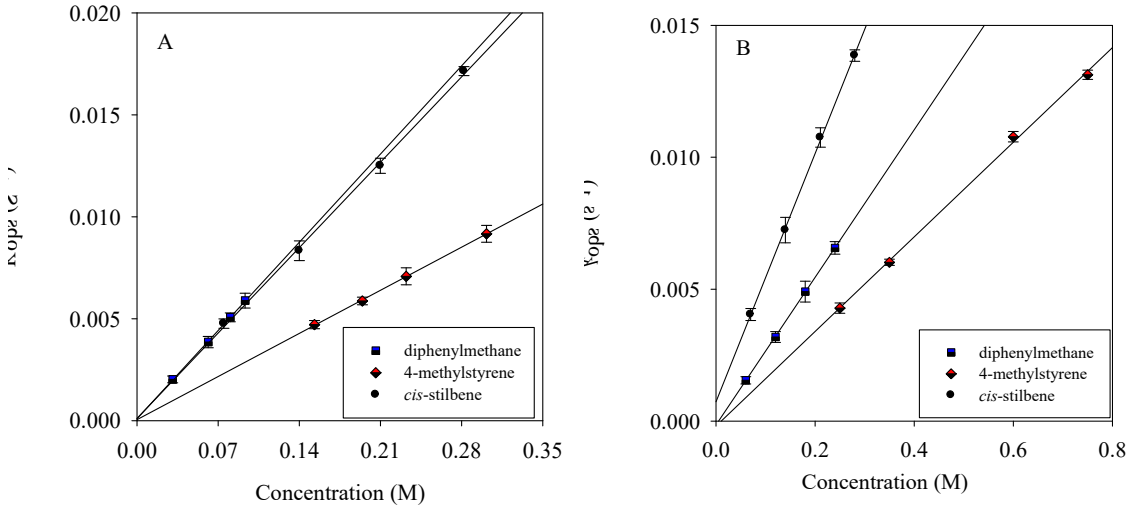

Figure 17. (A) Kinetic plots of the observed rate constants for the reaction of photo-generated **6a** versus the concentration of *cis*-stilbene, 4-methylstyrene and diphenylmethane; (B) Kinetic plots of the observed rate constants for the reaction of chemical-generated **6a** versus the concentration of *cis*-stilbene, 4-methylstyrene and diphenylmethane.

Table 1. Second-order rate constants for reactions of porphyrin-iron(IV)-oxo species **6**[a].

Substrate	$10^{-2} \times k_{ox}$ ($M^{-1}s^{-1}$)			
	O=Fe^{IV}(TDCPP)		O=Fe^{IV}(TDFPP)	
	6a[b]	**6a**[c]	**6b**[b]	**6b**[c]
cis-cyclooctene	2.6 ± 0.2	1.5 ± 0.7	2.2 ± 0.2	1.9 ± 0.1
styrene	1.9 ± 0.2	1.0 ± 0.1.4	1.5 ± 0.1	-
4-methylstyrene	3.1 ± 0.3	2.0 ± 0.2	2.4 ± 0.001	-
diphenylmethane	6.2 ± 0.5	2.8 ± 0.4	4.7 ± 0.1	-
cyclohexene	12 ± 2	11 ± 1	8.3 ± 0.5	-
ethylbenzene-d_{10}	0.84 ± 0.1	-	0.75 ± 0.4	0.71 ± 0.1

[a] In CH_3CN at 23±2 °C. The values are the average of 2-3 runs with 2σ.

[b] Photo-generated from this work.

[c] Chemical-generated by $PhI(OAc)_2$.

The photo-generated compound II (**6a**) in CH_3CN solution reacted with diphenylmethane and a second-order rate constant k_{ox} of (6.2 ± 0.5) × 10^{-2} $M^{-1}s^{-1}$ was obtained. A smaller k_{ox} of (2.8 ± 0.4) × 10^{-2} $M^{-1}s^{-1}$ was found in the reaction of chemical-generated **6a** with the same substrate. Other substrates used in the same system gave similar results comparing the photochemical and chemical methods. Another electron-deficient system (**6b**) was also used in a similar kinetic study, and the obtained

second-order rate constant gave similar kinetic results. The k_{ox} values shown in Table 2 provide a quantitative comparison of the kinetics of the same iron(IV)-oxo porphyrins generated by photochemical and chemical methods. As reported previously, laser flash photolysis techniques have been successfully developed for generation of a variety of high-valent transition metal-oxo species supported by porphyrinoid macrocycles. Furthermore, the kinetics of oxidation reactions of the photo-generated transients of interest are not convoluted with the kinetics of the reactions that form the transients by chemical methods.[31c] The photochemical method permit direct measurement of kinetics under single-turnover conditions.

4.3 Kinetic studies of sulfoxidation by photo-generated compound II models $[Fe^{IV}(Por)O]$ (**6a - 6b**)

In addition, the kinetics of oxidation of a series of thioanisoles by photo-generated **6a** and **6b** were also investigated in this study. The oxo (**6a)** (10 μM) species decayed much more rapidly in the presence of thioanisoles, reacting as fast as 30 seconds in a stopped-flow mixing unit. In kinetic measurements of **6a**, we monitored the decay of the Soret-band λ_{max} at 417 nm over the course of the reaction because the absorbance for the oxo (**6a)** species are stronger than the iron(III) product. As shown in Figure 18A, the time-resolved spectra show the clean conversion of **6a** to regenerate the iron(III) product. The isosbestic points at 407, 440, 532, 566 and 656 nm, demonstrate that the Fe^{IV}-oxo (**6a**) species were fully converted to the final Fe^{III} species without accumulation of any other intermediates. The Q-band absorbance at 570 nm of the regenerated iron(III)

product differs from 510 nm of **2a.** It indicates that the iron(III) porphyrin species contain hydroxide as the axial ligand, which has a distinct UV-vis spectra.[35] This may be taken as evidence that adventitious water in CH_3CN under the conditions that we employed was involved in the oxidation of **6a** and formation of iron(III)-containing product.

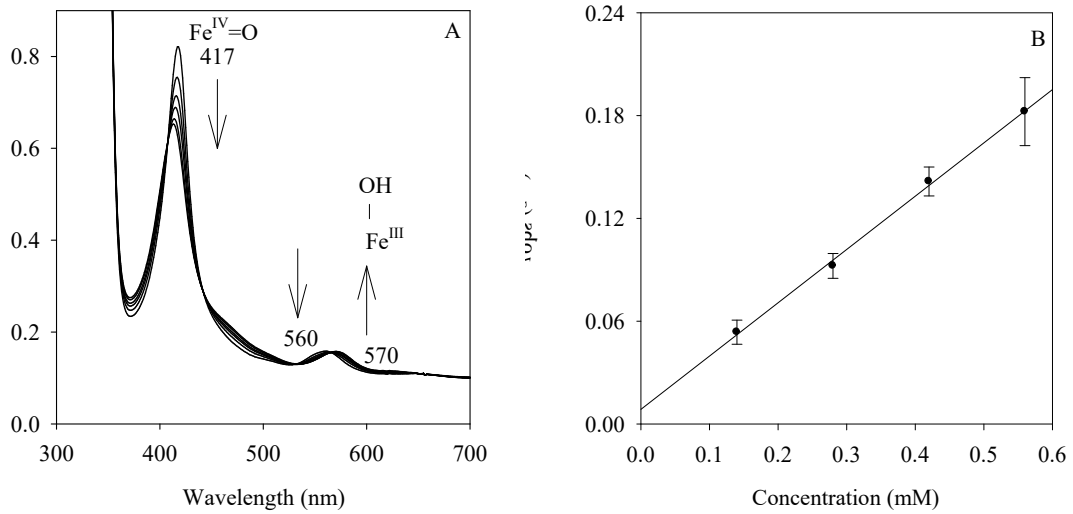

Figure 18. (A) Time-resolved spectra of photo-generated **6a** reacting in CH_3CN with thianisole (0.4 M) over 60 s. (B) Kinetic plot of the observed rate constants for the reaction of **6a** versus the concentration of thioanisole.

Photo-generated species **6a** at low concentrations were stable for hours in CH_3CN solutions. The pseudo-first-order decay rate constant is taken as a background rate constant (k_0) in the absence of substrate, presumable due to the reaction of **6a** with the solvent (CH_3CN) or organic impurities. After the thioanisole was added, the pseudo-first-order decay rate constants increased linearly with substrate concentration (Figure 18B). The kinetic plot for the reactions of **6a** with thioanisole is shown

graphically in Figure 18B, where a plot of k_{obs} versus the concentration of thioanisole increases linearly. The apparent second-order rate constants (k_{ox}) for oxidation with a series of thioanisoles and other representative substrates are collected in Table 2 for comparison.

Table 2. Second-order rate constants (k_{ox}) for reactions of porphyrin-iron-oxo species **6**[a].

Substrate	Rate constant ($M^{-1}s^{-1}$)	
	$O{=}Fe^{IV}$(TDCPP)	$O{=}Fe^{IV}$(TDFPP)
	6a[b]	**6b**[b]
thioanisole	$(3.3 \pm 0.2) \times 10^{2}$	$(8.6 \pm 1.8) \times 10^{1}$
4-fluorothioanisole	$(1.9 \pm 0.2) \times 10^{2}$	$(5.0 \pm 0.3) \times 10^{1}$
4-chlorothioanisole	$(9.1 \pm 0.4) \times 10^{2}$	$(8.7 \pm 0.4) \times 10^{1}$
4-methylthioanisole	$(9.3 \pm 0.1) \times 10^{2}$	$(1.1 \pm 0.1) \times 10^{2}$
4-methoxythioanisole	$(9.8 \pm 0.1) \times 10^{2}$	$(2.0 \pm 0.2) \times 10^{2}$
cis-stilbene	$(6.1 \pm 0.1) \times 10^{-2}$	$(4.0 \pm 0.1) \times 10^{-2}$
ethylbenzene	$(1.7 \pm 0.1) \times 10^{-1}$	$(1.5 \pm 0.1) \times 10^{-1}$

[a] In CH_3CN at 23 ± 2 °C. The values are the average of 2-3 runs with 2σ.

[b] Photo-generated from this work.

The second-order rate constants (k_{ox}) values determined from k_{obs} versus the concentration of substrate provide a quantitative measure of the remarkable rate acceleration of sulfide oxidation by compound II models. From the kinetic data shown in Table 2, the k_{ox} of alkene epoxidations in the ranges from $(6.1 \pm 0.1) \times 10^{-2}$ to $(6.1 \pm 0.4) \times 10^{-3}$ and the hydrocarbon hydroxylation rates in the ranges of $(4.4 \pm 0.3) \times 10^{-1}$ to $(3.7 \pm 0.2) \times 10^{-3}$ $M^{-1}s^{-1}$ (hydroxylation), are 3 to 4 orders of magnitude smaller than the k_{ox} determined for sulfoxidation reactions which are in the range from $(9.8 \pm 0.1) \times 10^{2}$ to $(3.7 \pm 0.3) \times 10^{1}$ $M^{-1}s^{-1}$. Such rate acceleration for sulfoxiations by **6a-b** clearly reflects the enhanced nucleophilicity and ease of oxidation of sulfur versus hydrocarbons.

In addition, the kinetic data in Table 1 and 2 show an inverted reactivity order for iron(IV)-oxo porphyrins (**6**) with all substrates. In general, one can observe that more electron-withdrawing ligands give more reactive metal-oxo derivatives in view of the electrophilic nature of high-valent metal-oxo complexes.[36] In the two porphyrin systems studied here, however, the reactivity order is inverted with the system of least electron demand, i.e. the TDCPP complex **6a** apparently reacting faster with any given substrate than the more electron-deficient **6b**. In consideration of their similar structure, photochemical and spectral behaviors, the different reactivities of **6a** and **6b** do not result from different mechanisms for their oxidation reactions. These kinetic results strongly support the previously proposed mechanistic model involving disproportionation of **6** to give the Fe^{III} product and a more reactive porphyrin-iron(IV)-oxo radical cationic species

(**8**) as the predominant oxidants in these systems (Scheme 11).[23b, 32a] In practice, the concentration of **8** might be too small to be observed, and the oxo **6** species are the major species which are observed . If complexes **8** are the true oxidants in the formation of these species, the equilibrium constants (k_{dis}) should be more favorable for the system with the least electron demand. The observed kinetic data indicate that the disproportionation equilibrium constant (k_{dis}) should be larger for the less electron-demanding TDCPP ligand; therefore, the populations of species **8** are controlled by the disproportionation equilibrium. Furthermore, a higher valence state of (+5) than the species **6** state of (+4), also provides a convenient "two-electron" oxo transfer reagent to oxidize substrate to regenerate iron(III) product instead of iron(II).

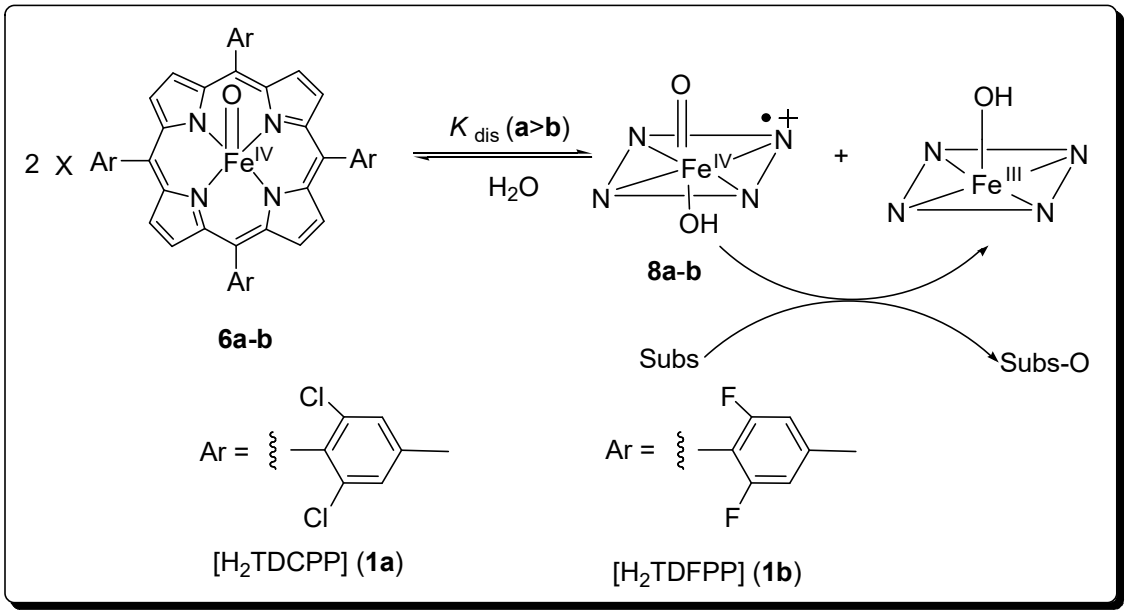

Scheme 14. A disproportionation pathway for reactions of species **6**.

The mechanistic model in Scheme 14 is similar to that proposed for reactions of neutral porphyrin–manganese(IV)-oxo[26d] and corrole-manganese(V)-oxo species,[28a, 37] where the actual oxidants in those systems apparently are cationic porphyrin–manganese(V)-oxo and corrole-manganese(VI)-oxo species, respectively, formed via a disproportionation mechanism. Importantly, direct conversion of **6a** to the compound I species **8a** in an acid-catalyzed reaction was reported.[38] This disproportionation mechanism also explains previous research that compound II species were more stable in alkaline solutions than in neutral or acidic solutions, owing to slow formation of reactive compound I in the absence of an acid catalyst.

4.4 Competition studies of sulfide oxidation reactions

In the catalytic oxidation for alkenes, activated hydrocarbons and organic sulfides with iron(III)porphyrin complexes, iodobenzene diacetate [$PhI(OAc)_2$] has been employed as the efficient oxygen source.[39] In the presence of a small amount of water, $PhI(OAc)_2$ is more efficient than the commonly used PhIO and other oxygen sources. In this study, we also found that iron(III) porphyrins catalyzed highly efficient oxidation of sulfides. Under optimized conditions, thioanisoles can be efficiently oxidized into sulfoxides, or sulfones by additional oxidation. The selectivity is simply determined by the amount of $PhI(OAc)_2$ (Scheme 15). Under usual catalytic conditions, $PhI(OAc)_2$ does not show appreciable reactivity towards organic sulfides nor damage the metal catalysts.

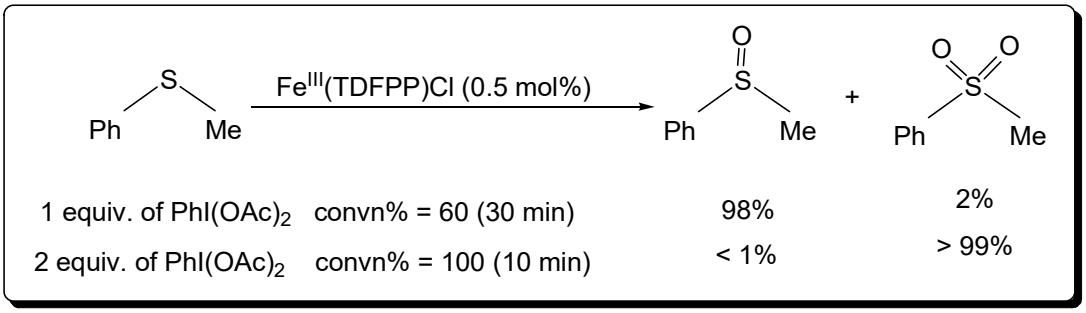

Scheme 15. Iron(III) porphyrin-catalyzed sulfide oxidations with $PhI(OAc)_2$.

$PhI(OAc)_2$ served as an efficient oxidant to oxidize the iron(III) complexes **2** to produce porphyrin-iron(IV)-oxo **6**. In the presence of substrate, oxo **6** decayed back to Fe^{III} product. The directly observed iron(IV)-oxo species **6** in the above kinetic studies are not necessarily the active oxidant under catalytic turnover conditions. The typical method to evaluate the activity of the same species in the two sets of conditions, is to compare the ratios of products formed under catalytic turnover conditions to the ratios of rate constants measured in direct kinetic studies.[27] If the same oxidant is present in the two cases, the ratios of absolute rate constants from direct measurements and relative rate constants from the competition studies should be similar. However, a coincident similarity for two different oxidants cannot be excluded. When the ratios are not similar, the active oxidants under the two sets of conditions should be different.

The competitive sulfoxidation reactions catalyzed by chloro-iron(III) porphyrin complexes (**2**) with $PhI(OAc)_2$ as a sacrificial oxygen source were also conducted. In this study, a limiting amount of sacrificial oxidant [$PhI(OAc)_2$] was used to keep the conversion less than 20%. The amounts of oxidation products formed were determined

by GC analysis. Based on the oxidant consumed each sulfide substrate was oxidized to give the corresponding sulfoxide with nearly quantitative yield without over-oxidation to the product sulfone. The ratios of absolute rate constants gained from the direct kinetic studies differed substantially from the oxidation ratios for competition oxidation reactions of the two substrates in the two systems (Table 3). These very unusual results were obtained from the oxidations of *para*-fluorothioanisole and ethylbenzene by iron(IV)-oxo **6**. The absolute rate constant for oxidation of *para*-fluorothioanisole by **6** is smaller than that for oxidation of thioaniolse by the same oxo species (Table 3), but *para*-fluorothioanisole is oxidized faster than thioanisole in competition studies with iron(III) porphyrins as the catalyst. One obvious explanation for this behavior is that a compound II species is unlikely to serve as the sole active oxidant under turnover conditions.

Table 3. Relative rate constants from kinetic studies and competition catalytic oxidation[a]

Porphyrin	Substrates	Method	k_{rel}[b]
TDFPP	*p*-F-PhSMe/PhSMe	Kinetic results	0.58
		$PhI(OAc)_2$	1.39
TDFPP	*p*-Cl-PhSMe/PhSMe	Kinetic results	1.0
		$PhI(OAc)_2$	1.10
TDFPP	*p*-Me-PhSMe/PhSMe	Kinetic results	1.29
		$PhI(OAc)_2$	1.87
TDFPP	*p*-MeO-PhSMe/PhSMe	Kinetic results	2.3
		$PhI(OAc)_2$	3.95
TDFPP	*cis*-stilbene/styrene	Kinetic results	3.27
		$PhI(OAc)_2$	1.98
TDFPP	styrene/ethylbenzene	Kinetic results	0.10
		$PhI(OAc)_2$	14.0
TDCPP	*p*-Me-PhSMe/PhSMe	Kinetic results	1.26
		$PhI(OAc)_2$	1.11

[a]A reaction solution containing equal amounts of two substrates, e.g., thioanisole (0.2 mmol) and substituted thioanisole (0.2 mmol), iron(III) porphyrin catalyst (1 μmol) and an internal standard of 1,2,4-trichlorobenzene was prepared in CH_3CN (0.5 mL).

Iodobenzene diacetate $PhI(OAc)_2$ (0.1 mmol) was added with 5 μL H_2O, and the mixture was stirred for ca. 5 to 10 min at 23 ± 2 °C.

[b]Relative ratios of absolute rate constants from kinetic results with iron(VI)-oxo porphyrin complexes and for competitive oxidations with various iron(III) porphyrin catalysts at ambient temperature. All competition ratios are averages of 2-3 determinations with standard deviations smaller than 10% of the reported values.

Further evidence that a different oxidant is involved in the catalytic oxidations instead of the iron(IV)-oxo complex is seen in the linear Hammett plot for competitive oxidations of the series of substituted thioanisoles (Y-thioanisole, Y = 4-MeO, 4-Me, 4-F, 4-Cl, and H). Figure 18 depicts a linear correlation (R = 0.98) of $\log k_{rel}$[k_{rel} = k(Y-thioanisole)/k(thioanisole)] versus Hammett σ+ substituent constant. The slope (ρ_+) of the plot is –0.67, which indicates transition states for rate-limiting steps which involve charge separation. Similarly, a linear Hammett plot with a larger slope (ρ_+ = –1.9) was observed for the reactivity of a porphyrin-iron(IV)-oxo radical cation with substituted styrene.[28b] Apparently, the competitive product studies and Hammett correlation analysis strongly suggest that the observed iron(IV)-oxo species is unlikely to be the oxidant. Indeed, the more reactive porphyrin-iron(V)-oxo radical cation as the premier reactive intermediate is plausible, even though it was not observed during the catalytic reactions.

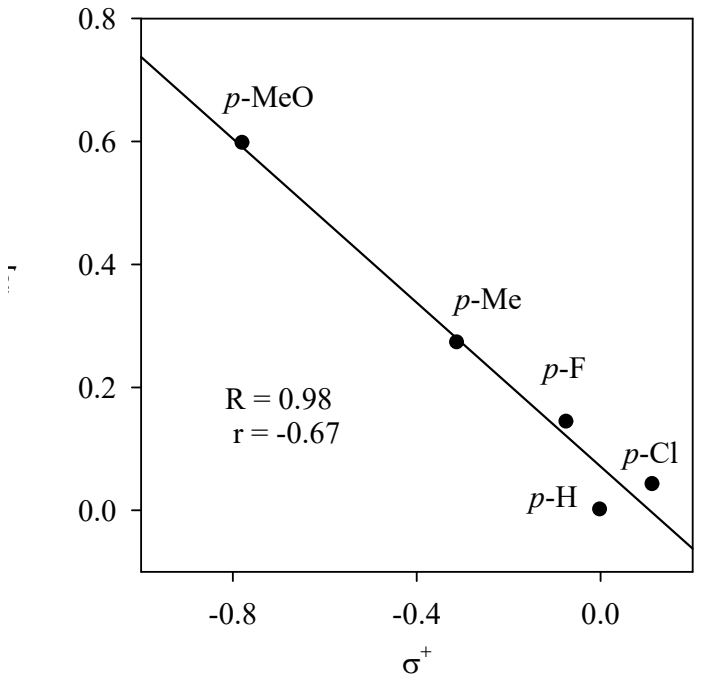

Figure 19. Hammett correlation studies (log *k*rel vs σ^+) for the Fe^{III}(TDFPP)Cl-catalyzed oxidation of substituted thioanisoles by $PhI(OAc)_2$ in CH_3CN at 23 ± 2 °C.

CHAPTER 5

CONCLUSION

In conclusion, a serious of iron(III) porphyrin and manganese(III) porphyrin complexes were successfully synthesized and spectroscopically characterized. By two different approaches, porphyrin iron(IV)-oxo (**6a** and **6b**) and porphyrin manganese(IV)-oxo (**7a** and **7b**) species were successfully generated in two electron-deficient ligand systems by photochemical and chemical methods. With $PhI(OAc)_2$ as external sacrificial oxidant, both of oxo **6** and **7** were produced by oxidation of Fe^{III}/Mn^{III} complexes. More importantly, the photochemical approach provides a new entry to access iron(IV)-oxo and manganese(IV)-oxo species (**6** and **7**), which permits direct detection and kinetic studies of the oxidations. In dilute solution, the iron(IV)-oxo porphyrin species are more stable than the corresponding manganese(IV)-oxo porphyrin species, which decayed quickly back to Mn^{III} precursors.

The oxidation kinetics of active hydrocarbons, alkenes and sulfide by photo- and chemical-generated porphyrin-iron(IV)-oxo complexes (**6**) were conducted in the two electron-deficient systems. The kinetic data in this study reveals the sulfide oxidation reactions are 3 to 4 orders of magnitude faster than alkene epoxidation and activated C-H bond hydroxylation reactions. The order of reactivity for compound II (**6a** and **6b**) in the oxidation of hydrocarbonds, alkenes and sulfides, is inverted as expected for electrophilic

metal-oxo oxidants. These observations indicate that hydroxylation, epoxidation and sulfoxidation by these iron(IV)-oxo species presumably occurs through a disproportionation mechanism to produce higher oxidized iron-oxo complexes as the true oxidant. The competition product studies and Hammett correlation analysis confirmed that the observed iron(IV)-oxo species are unlikely to be the oxidant for the catalytic oxidations by iron(III) porphyrin catalysts and $PhI(OAc)_2$. Indeed, the more reactive iron(IV)-oxo-porphyrin radical cation was indicative as the premier reactive intermediate, even though it was not observed during the catalytic reaction.

REFERENCES

1. Ortiz de Montellano, P. R., *Cytochrome P450 Structure, Mechanism, and Biochemistry*. 3rd ed.; Kluwer Academic/Plenum: New York, 2005.

2. Sheldon, R. A., *Metalloprophyrins In Catalytic Oxidations*. Marcel Dekker: New York, 1994.

3. (a) Brink, G. T., Green, Catalytic Oxidation of Alcohols in Water. *Science* **2000,** *287* (5458), 1636-1639; (b) Groves, J. T., Shalyaev, K.; Lee, J., Oxometalloporphyrins in Oxidative Catalysis. In *The Porhyrin Handbook*, Kadish, K. M. S., K. M.; Guilard, R., Ed. 2000; Vol. 4, pp 17-40.

4. (a) Punniyamurthy, T.; Velusamy, S.; Iqbal, J., Recent Advances in Transition Metal Catalyzed Oxidation of Organic Substrates with Molecular Oxygen. *Chem.Rev.* **2005,** *105* (6), 2329-2363; (b) Zhang, R.; Vanover, E.; Chen, T.-H.; Thompson, H., Visible light-driven aerobic oxidation catalyzed by a diiron(IV) μ-oxo biscorrole complex. *Appl. Catal. A* **2013,** *465*, 95-100.

5. (a) Guengerich, P. F., Common and Uncommon Cytochrome P450 Reactions Related to Metabolism and Chemical Toxicity. *Chemical Research in Toxicology* **2001,** *14* (6), 611-650; (b) Ortiz de Montellano, P. R. D. V., J. J.,, Oxidizing species in the mechanism of cytochrome P450. *Nat. Prod* **2002,** *19*, 477-493.

6. Zhang, R., Asymmetric Organic Oxidation by Chiral Ruthenium Complexes Containing D2- and D4- Symmetric Porphyrinato Ligands. *Ph. d. Thesis* **2000**, 1-235.

7. Sono, M.; Roach, M. P.; Coulter, E. D.; Dawson, J. H., Heme-Containing Oxygenases. *Chem. Rev.* **1996,** *96* (7), 2841-2887.

8. Poulos, T. L. F., B. C.; Howard, A. J.;, High-Resolution Crystal Structure of Cytochrome P450cam. *Journal of Molecular Biology* **1987,** *195*, 687-700.

9. Omura, T. S., R.;, A new cytochrome in liver microsomes. *Biol. Chem* **1962,** *237*, 1376-1376.

10. Denisov, I. G.; Makris, T. M.; Sligar, S. G.; Schlichting, I., Structure and chemistry of cytochrome P 450. *Chem. Rev.* **2005,** *105* (6), 2253-2277.

11. (a) Newcomb, M.; Zhang, R.; Chandrasena, R. E. P.; Halgrimson, J. A.; Horner, J. H.; Makris, T. M.; Sligar, S. G., Cytochrome P 450 compound I. *J. Am. Chem. Soc.* **2006,** *128* (14), 4580-4581; (b) Zhang, R.; Nagraj, N.; Lansakara-P, D. S. P.; Hager, L. P.; Newcomb, M., Kinetics of Two-Electron Oxidations by the Compound I Derivative of Chloroperoxidase, a Model for Cytochrome P450 Oxidants. *Org. Lett.* **2006,** *8* (13), 2731-2734.

12. Groves, J. T., Reactivity and Meschanisms of Metalloporphyrin-Catalyzed Oxidations. *J. Porph. Phthal* **2000,** *4*, 350-352.

13. (a) Meunier, B., *Metal-Oxo and Metal-Peroxo Species in Catalytic Oxidations*. Springer-Verlag: Berlin, 2000; (b) Meunier, B., Metalloporphyrins as Versatile Catalysts for Oxidation Reactions and Oxidative DNA Cleavage. *Chem. Rev.* **1992,** *92* (6), 1411-1456; (c) Chen, C. M. H., J. S.,, Metalloporphyrin-based oxidation systems: from

biomimetic reactions to application in organic synthesis. *Chem. Commum* **2009**, 2336-4015.

14. (a) Krebs, C. G. F., D.; Walsh, C. T.; Bollinger, J. M., , Non-heme Fe(IV)-Oxo Intermediates. *Acc. Chem. Res.,* **2007,** *40 (7)*, 484-492; (b) Watanabe, Y.; Fujii, H., Characterization of High-Valent Oxo-Metalloporphyrins. In *Metal-Oxo and Metal-Peroxo Species in Catalytic Oxidations*, Meunier, B., Ed. Springer-Verlag: Berlin, 2000; (c) Costas, M.; Mehn, M. P.; Jensen, M. P.; Que, L., Dioxygen Activation at Mononuclear Nonheme Iron Active Sites: Enzymes, Models, and Intermediates. *Chem. Rev.* **2004,** *104*, 939-986.

15. Jung, C. S.; V. Lendzian, F., Freeze-quenched iron-oxo intermediates in cytochromes P450. *Biochem. Biophys. Res. Commun.* **2005,** *338*, 355-364.

16. (a) Raner, G. M. H., A. J.; Morton, R. E.; Ballou, D. R; Coon, M. J., , Stopped-flow spectrophotometric analysis of intermediates in the peroxo-dependent inactivation of cytochrome P450 by aldehydes. *Inor. Biochem.* **2000,** *81*, 153-160; (b) Newcomb, Highly reactive electrophilic oxidants in cytochrome P450 catalysis. . *biochem. Biophys. Commun* **2005**, 338, 394-403.

17. Dey, A.; Ghosh, A., "True" iron(V) and iron(VI) porphyrins: a first theoretical exploration. *J. Am. Chem. Soc.* **2002,** *124* (13), 3206-7.

18. Groves, J. T.; Haushalter, R. C.; Nakamura, M.; Nemo, T. E.; Evans, B. J., High-valent iron-porphyrin complexes related to peroxidase and cytochrome P-450. *J. Am. Chem. Soc.* **1981,** *103* (10), 2884-6.

19. (a) Pennerhahn, J. K. M., T. J.; Rentier, M.; Balch, A.L.; Groves, J. T.; Dawson, J. H.; Hodgson, K. O., , structureal characterization of horseradish peroxidase using EXAFS spectroscopy. Evidence for Fe=O ligation in compounds I and II. . *Am. Chem. Soc.* **1986,** *108*, 7819-7825; (b) Pennerhahn, J. E. M., T. J.; Renner, M.; Latosgrazynsky, L.; K. S.; Davis, I. M.; Balch, A. L.; Groves, J. T.; Dawson, J. H.; Hodgson, K. O., , X-ray absorptionspectroscopic studies of high balent iron porphyrins. Horseradish peroxidase compound I and II and synthetic models. *Biol. Chem* **1983,** *258*, 12761-12764; (c) Groves, J. T. Q., R.; mcmurry, T.J.; Lang, g; Boso, B., , Iron(IV) porphyrins from iron(III) porphyrin cation radicals. *Chem. Soc, Chem. Commum.* **1984,** *31*, 4404-4409.

20. Mandon, D. W., R.; jayaraj, K.; Gold, A.; Terner, J.; Bill, E.; Trautwein, A. X., , Models for peroxidase compound I: generation and spectroscopic characterization of new oxoferryl porphyrin .pi. cation radical species. *Inorg. Chem.* **1992,** *31*, 4404.

21. Gold, A. J., K.; Doppelt, P.; Weiss, R.; Chottard, G; Bill, E.; Ding, X.; Trautwein, A. X., , Oxoferryl complexes of the halogenated (porphinato)iron catalyst [tetrakis(2,6-dichlorophenyl)porphinato]iron. *Am. Chem. Soc.* **1988,** *110*, 5756-5761.

22. Chin, D.-H.; La Ma., G. N.; Balch, A. L., Role of ferryl (FeO2+) complexes in oxygen atom transfer reactions. Mechanism of iron(II) porphyrin catalyzed oxygenation of triphenylphosphine. *J. Am. Chem. Soc.* **1980,** *102*, 5945-5947.

23. (a) Dawson, J. H., Probing structure-function relations in heme-containing oxygenases and peroxidases. *Science* **1988,** *240* (4851), 433-9; (b) Groves, J. T.; Gross, Z.; Stern, M. K., Preparation and Reactivity of Oxoiron(IV) Porphyrins. *Inorg. Chem.*

1994, *33* (22), 5065-72; (c) Oszajca, M.; Franke, A.; Drzewiecka-Matuszek, A.; Brindell, M.; Stochel, G.; van Eldik, R., Temperature and Pressure Effects on C−H Abstraction Reactions Involving Compound I and II Mimics in Aqueous Solution. *Inorg. Chem.* **2014,** *53*, 2848-2857.

24. Groves, J. T.; Lee, J.; Marla, S. S., Detection and Characterization of an Oxomanganese(V) Porphyrin Complex by Rapid-Mixing Stopped-Flow Spectrophotometry. *J. Am. Chem. Soc.* **1997,** *119* (27), 6269-6273.

25. (a) Suslick, K. S.; Watson, R. A., Photochemical reduction of nitrate and nitrite by manganese and iron porphyrins. *Inorg. Chem.* **1991,** *30* (5), 912-19; (b) Suslick, K. S.; Watson, R. A., The photochemistry of chromium, manganese, and iron porphyrin complexes. *New J. Chem.* **1992,** *16* (5), 633-42; (c) Maldotti, A.; Molinari, A.; Amadelli, R., Photocatalysis with Organized Systems for the Oxofunctionalization of Hydrocarbons by O2. *Chem. Rev.* **2002,** *102*, 3811-3836.

26. (a) Harischandra, D. N.; Zhang, R.; Newcomb, M., Photochemical Generation of a Highly Reactive Iron-Oxo Intermediate. A True Iron(V)-Oxo Species? *J. Am. Chem. Soc.* **2005,** *127* (40), 13776-13777; (b) Pan, Z.; Wang, Q.; Sheng, X.; Horner, J. H.; Newcomb, M., Highly Reactive Porphyrin−Iron−Oxo Derivatives Produced by Photolyses of Metastable Porphyrin−Iron(IV) Diperchlorates. *J. Am. Chem. Soc.* **2009,** *131* (7), 2621-2628; (c) Pan, Z.; Zhang, R.; Fung, L. W. M.; Newcomb, M., Photochemical Production of a Highly Reactive Porphyrin-Iron-Oxo Species. *Inorg. Chem.* **2007,** *46* (5), 1517-1519; (d) Zhang, R.; Horner, J. H.; Newcomb, M., Laser Flash

Photolysis Generation and Kinetic Studies of Porphyrin-Manganese-Oxo Intermediates. Rate Constants for Oxidations Effected by Porphyrin-MnV-Oxo Species and Apparent Disproportionation Equilibrium Constants for Porphyrin-MnIV-Oxo Species. *J. Am. Chem. Soc.* **2005,** *127* (18), 6573-6582.

27. Zhang, R.; Newcomb, M., Laser Flash Photolysis Generation of High-Valent Transition Metal-Oxo Species: Insights from Kinetic Studies in Real Time. *Acc.Chem. Res.* **2008,** *41* (3), 468-477.

28. (a) Zhang, R.; Harischandra, D. N.; Newcomb, M., Laser flash photolysis generation and kinetic studies of corrole-manganese(V)-oxo intermediates. *Chem. Eur. J.* **2005,** *11* (19), 5713-5720; (b) Zhang, R.; Newcomb, M., Laser Flash Photolysis Formation and Direct Kinetic Studies of Manganese(V)-Oxo Porphyrin Intermediates. *J. Am. Chem. Soc.* **2003,** *125* (41), 12418-12419.

29. Lindsey, J.; Wagner, R. D., Investigation of the synthesis of ortho-substituted tetraphenylporphyrins. *J. Org. Chem.* **1989,** *54*, 828-836.

30. Adler, A. D.; Longo, F. R.; Finarelli, J. D.; Goldmacher, D.; Assour, J.; Korsakoff, L., A simplified synthesis of meso-tetraphenylporpyrin. *J. Org. Chem.* **1967,** *32*, 476.

31. (a) Nam, W., High-Valent Iron(IV)–Oxo Complexes of Heme and Non-Heme Ligands in Oxygenation Reactions. *Acc. Chem. Res.,* **2007,** *40* (7), 522-531; (b) Wallar, B. J.; Lipscomb, J. D., Dioxygen activation by enzymes containing binuclear non-heme iron clusters. *Chem. Rev.* **1996,** *96* (7), 2625-2657; (c) Fujii, H., Electronic structure and reactivity of high-valent oxo iron porphyrins. *Coord. Chem. Rev.* **2002,** *226*, 51-60; (d) S.

P. de Visser, W. N., in: K. M. Kadish, K. M. Smith, R. Guilard (Eds.), , Handbook of porphyrin science, . *World scientific publishing, Singapore* **2010**, 85-139; (e) McDonald, A. R.; Que, L., High- valent nonheme iron- oxo complexes: Synthesis, structure, and spectroscopy. *Coord. Chem. Rev.* **2013,** *257*, 414-428.

32. (a) Pan, Z.; Newcomb, M., Kinetics and mechanism of oxidation reactions of porphyrin-iron(IV)-oxo intermediates. *Inorg. Chem.* **2007,** *46*, 6767-6774; (b) Nam, W.; Park, S. E.; Lim, I. K.; Lim, M. H.; Hong, J.; Kim, J., First direct evidence for stereospecific olefin epoxidation and alkane hydroxylation by an oxoiron(IV) porphyrin complex. *J. Am. Chem. Soc.* **2003,** *125*, 14674-14675.

33. (a) Kwong, K. W. P., D.; Malone, J.; Lee, N. F.; Kash, B.; Zhang, R.;, An investigation of ligand effects on the visible light-induced formation of porphyrin–iron(IV)-oxo intermediates. *New J. Chem.* **2017,** *41*, 14334-14341; (b) Chen, T. H.; Asiri, N.; Kwong, K. W.; Malone, J.; Zhang, R., Ligand control in the photochemical generation of high-valent porphyrin-iron–oxo derivatives. *Chem. Commun.* **2015,** *51*, 9949-9952.

34. Pan, Z.; Zhang, R.; Newcomb, M., Kinetic studies of reactions of iron(IV)-oxo porphyrin radical cations with organic reductants. *J. Inorg. Biochem.* **2006,** *100* (4), 524-532.

35. Machii, K. W., Y.; Morishima, I.;, Acylperoxo-Iron(III) Porphyrin Complexes: A New Entry of Potent Oxidants for the Alkene Epoxidation. *J. Am. Chem. Soc.* **1995,** *117* (25), 6691-6697.

36. Dolphin, D.; Traylor, T. G.; Xie, L. Y., Polyhaloporphyrins: Unusual ligands for metals and metal-catalyzed oxidations. *Acc. Chem. Res.* **1997,** *30* (251-259).

37. Kwong, K. W.; Lee, N. F.; Ranburg, D.; Malone, J.; Zhang, R., Visible light-induced formation of corrole-manganese(V)-oxo complexes: Observation of multiple oxidation pathways. *J. Inorg. Biochem.* **2016,** *163*, 39-44.

38. Pan, Z. N., M.; , Acid-catalyzed disproportionation of oxoiron(IV) porphyrins to give oxoiron(IV) porphyrin radical cations. *Inorg. Chem. Commun.* **2011,** *14* (6), 968-970.

39. (a) In, J. H.; Park, S. E.; Song, R.; Nam, W., Iodobenzene diacetate as an efficient terminal oxidant in iron(III) porphyrin complex-catalyzed oxygenation reactions. *Inorg. Chim. Acta* **2003,** *343*, 373-376; (b) Chen, T.-H.; Kwong, K.-W.; Carver, A.; Luo, W. L.; Zhang, R., Enhanced iron(III) corrole-catalyzed oxidations with iodobenzene diacetate: Synthetic and mechanistic investigations. *Appl. Catal. A* **2015,** *497*, 121-126.

RESUME

Haiyan Liu

Haiyanliu2018@gmail.com

270-723-7206

EDUCATION

- ✧ M. S. in Chemistry: Western Kentucky University, KY, USA, 2016 − 2018
  - ✧ Thesis: Synthesis and Kinetic Studies of High-Valent Metal-Oxo Species Generated by Photochemical and Chemical Methods.
- ✧ M. S. in Logistics Engineering: Shanghai Jiao Tong University, China, 2006 − 2009
  - ✧ Thesis: Model for Advanced Bonded and Supervised Warehouse
- ✧ B. S. in Chemistry Education: Lingnan Normal University, 1994 − 1998

WORKING EXPERIENCE

- ✧ Teaching Assistant, Western Kentucky University, Bowling Green, Kentucky, USA, 2016 − present
- ✧ Marketing Manager, Xianggen Cosmetics Packaging Co. Ltd., Shenzhen, China, 2010 − 2015

- ✧ Assistant Manager of Export Supervised Warehouse, Hongkai Logistics Co. Ltd., Shenzhen, China, 2004 − 2010
- ✧ Marketing/Sales, Longxiang International Trading Co. Ltd., Shanghai, China, 2000 - 2004
- ✧ Chemisty Teacher, Zhongshan (East District) High School, Zhongshan, China, 1998 − 2000

PUBLICATIONS/PRESENTATIONS

- ✧ Ngo Fung Lee; Dharmesh Patel; Haiyan Liu and Rui Zhang. Insights from Kinetic Studies of Photo-generated Compound II Models: Reactivity toward Aryl Sulfides. *J. Inorg. Biochem.* **2018**, 183, 58-65.
- ✧ Haiyan Liu; Yifei Zhao. New Model for Bonded warehouse. *Nanfang Journal Logistic engineering* (2008), 212-227
- ✧ Haiyan Liu; Dharmesh Patel; Rui Zhang (poster). "Kinetic Studies of Iron(IV)-Oxo Porphyrin Generated by Photochemical and Chemical Methods". 103th Annual Meeting of the Kentucky Academy of Science, 2017, Murray, KY.
- ✧ Haiyan Liu, Ngo Fung Lee and Rui Zhang (oral)." Synthesis and Kinetic Studies of High-Valent Metal-Oxo Species Generated by Photochemical and Chemical Methods". WKU Student Research Conference, Bowling Green, Ky, March 2018

HONORS/AWARDS

- ✧ 1st place in the contest of Management strategy for warehousing, 2008
- ✧ Teacher of Zhongshan City, 1999
- ✧ Undergraduate Student Scholarship, 1994 − 1998

ABBREVIATIONS AND SYMBOLS

Ar	Aryl
$BF_3 \cdot OEt_2$	Boron trifluoride diethyl etherate
CYP450s	Cytochrome P450 enzymes
DDQ	2,3-Dichloro-5,6-dicyano-p-benzequinone
DMF	*N, N*-Dimethylformamide
Fe^{III}(Por)Cl	Iron(III) porphyrin chloride
Mn^{III}(Por)Cl	Manganese(III) porphyrin chloride
Fe^{III}(TDCPP)Cl	Iron(III) 5,10,15,20-tetrakis(2,6-dichlorophenyl) porphyrin chloride
Fe^{III}(TDFPP)Cl	Iron(III) 5,10,15,20-tetrakis(2,6-difluorophenyl) porphyrin chloride
Mn^{III}(TDCPP)Cl	Manganese(III)5,10,15,20-tetrakis(2,6-dichlorophenyl) porphyrin chloride
Mn^{III}(TDFPP)Cl	Manganese(III)5,10,15,20-tetrakis(2,6-difluorophenyl) porphyrin chloride

$Fe^{III}(TMP)Cl$	Iron(III) 5,10,15,20-tetramesitylporphyrin chloride
^{1}H-NMR	Proton nuclear magnetic resonance
UV-vis	Ultraviolet-visible
$H_2(TMP)$	5,10,15,20-Tetramesitylporphyrin
$H_2(TDCPP)$	5,10,15,20-Tetrakis(2,6-dichlorophenyl) porphyrin
$H_2(TDFPP)$	5,10,15,20-Tetrakis(2,6-difluorophenyl) porphyrin
GC-MS	Gas chromatography-mass spectrometry
TPP	*meso*-Tetraphenylporphyrin
k_0	Background rate constant
k_{obs}	Observed pseudo-first-order rate constant
k_{ox}	Second-order rate constant
m-CPBA	*meta*-Chloroperoxybenzoic acid
PhIO	Iodosylbenzene
$PhI(OAc)_2$	Iodobenzene diacetate